ANTAGONISM BETWEEN TRASTUZUMAB AND ONCOLYTIC VSV IS OVERCOME BY CONJUGATION TO A MICROTUBULE DESTABILIZER

By

Vanessa Garcia

A thesis submitted in partial fulfillment of the requirements for the degree of Master of Science, Specialization in Biochemistry

University of Ottawa

Faculty of Medicine

Department of Biochemistry, Microbiology, and Immunology

July 16th, 2015

Supervisors:

Jean-Simon Diallo, PhD

Michael McBurney, PhD

ABSTRACT

HER2 overexpression is associated with poor breast cancer prognosis and increased risk of metastasis. Current HER2 targeted therapies include monoclonal antibody based strategies which work by reducing HER2 levels at the cell surface (trastuzumab), by preventing HER2 dimerization (pertuzumab), or via targeted delivery of a cytotoxic payload (trastuzumab emtansine). Although these therapies are successful in some cases, acquired and inherent resistance to these therapeutics remain a treatment hurdle. Oncolytic viruses (OVs) specifically target and lyse cancer cells while leaving normal cells unharmed. One such OV, VSVΔ51, replicates in interferon (IFN) defective cells, a characteristic of approximately 70% of tumours. We hypothesized that the combination of HER2 targeting therapies with VSVΔ51 could improve therapeutic efficacy. We found that HER2 overexpression was associtated with increased virus sensitivity and that modulation of HER2 signaling through a subset of activating ligands and inhibitory drugs could influence infection. We further established that the HER2 monoclonal antibodies trastuzumab and pertuzumab mediate an anti-viral effect on VSVΔ51 spread. Finally, we demonstrate that conjugation of a microtubule targeting agent to trastuzumab can overcome the induced anti-viral state and enhance VSVΔ51 spread specifically in cancer cells. Overall, this work highlights the importance of HER2 signaling and activation on VSVΔ51 spread and shows that conjugation of microtubule destabilizing agents to monoclonal antibodies can enhance VSVΔ51 efficacy.

ACKNOWLEDGEMENTS

I am very fortunate to have many people to thank for their help and support. First, I would like to thank my supervisor, Jean-Simon Diallo, whose leadership, insights, and motivation have been instrumental in my development as a researcher these past 4 years. Second, to the Diallo lab team members who have been an exceptional group of colleagues and friends; thank you to Rozanne and Nicole for their valuable research ideas and suggestions, to fellow students Ramya, MOhammed, Colin, Oliver, Nader, and Connie whose friendship and discussions I appreciate, to Jason, Jeff and Naveen for providing comedic relief, and finally to Andrew for helping me with *in vivo* experiments. I'd also like to acknowledge fellow past and present Bell, Atkins, and Auer lab members: Marie-Claude, Dom, Vicki, Carolina, Fabrice, Laura, Naomi, Monica, Jovian, Monique, Catia, Brian, Theresa, Casey, Katherine, Jiqing, Christiano, and Almo for their advice and support.

Je tiens aussi à remercier ma famille ici à Ottawa; mes grands-parents Bernard et Aline, mon oncle Robert et ma tante Louise qui sont toujours prêts à jouer aux cartes, me passer des mots d'encouragement ou encore des bons conseils. Merci à vous tous pour votre amour et pour les beaux moments que nous passons; la semaine ne serait complète sans un souper ensemble!

¿Y qué decir de mi familia? ¡No sé ni dónde empezar; gracias a los tres, lo que escribo no puede describir lo profundo de mis sentimientos! A mis padres Monique y Alfonso con quienes siempre puedo contar y que siempre me han impulsado a mayores alturas. A mi hermana Amanda que me conoce mejor que nadie y que siempre sabe como hacerme reír. ¡Los quiero muchisisimo!

TABLE OF CONTENTS

LIST OF ABBREVIATIONS

ADC= antibody-drug conjugate

ADCC= antibody-dependent cell-mediated cytotoxicity

AKT= protein kinase B

APC= anaphase promoting complex

AP-1= activating protein-1

BCL-XL= B-cell lymphoma extra-large

C/EBP-β= CCAAT/enhancer-binding protein-β

CDC20= cell division control protein 20

CDK1= cyclin dependent kinase 1

CLEOPATRA= Clinical Evaluation of Pertuzumab and Trastuzuamab Trial

CM= conditioned media

CPS II= carbamoyl phosphate synthetase II

DMEM= Dubelcco's modified Eagle's medium

DM1= derivative of maytansine 1

EGF= epidermal growth factor

EGFR= epidermal growth factor receptor

ELISA= enzyme-linked immunosorbent assay

ERK= extracellular signal-regulated kinase

FBS= fetal bovine serum

Fc= fragment crystallisable

FDA= Food and Drug Administration

GDP= guanosine-5'-diphosphate

GSK3β= glycogen synthase kinase-3β

GTP= guanosine-5'-triphosphate

HER= human epidermal growth factor receptor

HDAC= histone deacetylase

HSV-1= herpes simplex virus-1

IFN= interferon

IL-1β= interleukin-1β

IV= intravenous

IT= intratumoural

LDL= low-density lipoprotein

MAPK= mitogen-activated protein kinase

MBC= metastatic breast cancer

MCC= 4-[N-maleimidomethyl]-cyclohexane-1-carbonyl

MDA= microtubule destabilizing agent

MOI= multiplicity of infection

MMAE= monomethyl auristatin E

MSA= microtubule stabilizing agent

MT= microtubule

MTA= microtubule targeting agent

MTD= maximum tolerated dose

mTOR= mammalian target of rapamycin

NBF= neutral buffered formalin

NLRP3= NOD-like receptor family, pyrin domain containing 3

OV= oncolytic virus

PBS= phosphate-buffered saline

PCR= polymerase chain reaction

PDK-1 = Phosphoinositide-dependent kinase-1

PFS= progression free survival

PFU= plaque forming unit

PIP_2= phosphatidylinositol-4, 5-biphosphate

$PIP_{3=}$ phosphatidylinositol-3, 4, 5-triphosphate

PI3K= phosphoinositide 3-kinase

PS= phosphatidylserine

RIG-I= retinoic acid-inducible gene 1

RNP= ribonucleoprotein

RPMI= Roswell Park Memorial Institute medium

SAHA= suberanilohydroxamic acid

SC= subcutaneous

TGF-α= tumour growth factor-α

TK= tyrosine kinase

TKI= tyrosine kinase inhibitor

T-VEC= talimogene laherparepvec

VEGF= vascular endothelial growth factor

VSV= Vesicular stomatitis virus

VSe= viral sensitizer

LIST OF FIGURES AND ILLUSTRATIONS

1-INTRODUCTION

1.1-HISTORY OF VIRUSES AS CANCER THERAPEUTICS

The use of viruses as cancer therapeutics stemmed from case studies in the late 19th to early 20th century which described tumour regression following an acquired virus infection. One of the earliest reports, written in 1896, gave an account of a 42 year old woman whose leukemia went into a brief remission following an apparent influenza infection (Dock, 1904). Additional reports have described similar tumour regressions with chicken pox, West Nile, and more recent reports have noted such effects on leukemia and lymphoma in the presence of a measles infection (Bierman et al., 1953; Pasquinucci, 1971; Southam and Moore, 1951; Taqi et al., 1981). These case reports suggested that under certain circumstances some viruses could cause temporary tumour regression in patients and supported the idea of using viruses as cancer therapeutics.

Initial efforts in the development of virus based therapies were hampered by limitations in available tissue culture techniques which made it difficult to propagate, characterize, and screen potential viruses (Alemany, 2013). Subsequent advances of tissue and cell culture techniques allowed for screening of non-human animal viruses, which could overcome the problems associated with pre-existing anti-viral immunity, and identified two non-pathogenic Herpes viruses as causing cell death in a panel of human cancer cell lines (Hammon et al., 1963; Yohn et al., 1968). Further efforts by Southam and Moore contributed to the development of oncolytic virus therapy but were set aside in the 1960s during which time chemotherapeutic agents were widely adopted as the standard of care in cancer treatment (DeVita and Chu, 2008; Southam and Moore, 1952). The re-emergence of oncolytic viruses in the 1990s can be attributed to the progress of genetic engineering allowing for the manipulation of viral genomes

to, among other things, increase their oncolytic potential, improve tumour selectivity, and/or encode transgenes (Kelly and Russell, 2007).

1.2-ONCOLYTIC VIRUSES

Oncolytic viruses (OVs) can be broadly described as viruses with the ability to infect, replicate in, and kill cancer cells while leaving normal cells unharmed (Kelly and Russell, 2007). OVs are multimodal cancer therapeutics as they can induce cancer cell death using multiple mechanisms. They can induce durable anti-tumour immune responses by engaging the host's innate and adaptive immune system thus overcoming the immunosuppressive environment established by the tumour (Stojdl et al., 2003). Additionally, OVs can mediate a tumour specific vascular shutdown limiting blood flow leading to pervasive necrosis and apoptosis (Breitbach et al., 2007; Breitbach et al., 2011). Finally, OV replication often relies on defects or alterations in a cancer cell's signaling pathways. Defects in cellular thymidine kinase and interferon are among the defective pathways exploited by OV vaccinia virus and vesicular stomatitis virus (VSV), respectively (Alemany, 2013; Parato et al., 2005). Alterations that allow the cancer cell to resist apoptosis often make them susceptible to direct lysis by OVs, granting the virus a replicative niche (Ilkow et al., 2014; Mahoney and Stojdl, 2013).

1.2.1- ONCOLYTIC RHABDOVIRUSES: VSV

VSV is an arthropod-borne virus typically affecting cattle, swine, horses, and rodents (Russell, 2002). VSV infections in humans are rare, usually asymptomatic and typically restricted to agricultural and laboratory workers (Reif et al., 1987; Webb et al., 1987). In symptomatic cases, mild flu-like symptoms have been described and one case of viral encephalitis was reported in a 3 year old child in Panama (Quiroz et al., 1988). Pre-existing immunity to VSV is rare and is typically restricted to farming contexts (Tesh et al., 1969), an

advantage when considering its use as an OV since virus neutralization by host antibodies can hamper virus delivery to the tumour (Parato et al., 2005).

The small 11kb VSV genome encodes five genes and is composed of a single negative strand of RNA (Regan and Whittaker, 2013). VSV's broad tropism can be attributed to the glycoprotein (G protein) which binds phosphatidylserine (PS), a common component of cell-surface membranes, as well as the low-density lipoprotein (LDL) receptor (Finkelshtein et al., 2013). The G protein is also responsible for binding of the virus to the host cell and release of the viral genome in the cytoplasm via the endocytic pathway (Hastie et al., 2013). VSV replication occurs in the cytoplasm and is mediated by the ribonucleoprotein (RNP) complex composed of polymerases L and P as well as nucleocapsid (N) proteins. The L protein encodes an RNA dependent RNA polymerase and is also responsible for capping, methylation, and polyadenylation of viral transcripts, while the P protein is a polymerase co-factor facilitating transcription of viral mRNAs. The N protein is required for encapsidation of genomic RNA and is not involved in RNA synthesis (Hastie et al., 2013). Cytoplasmic viral replication does not allow for genetic recombination or integration of viral genes into the host cell and is an important safety factor for treatment of patients (Lichty et al., 2004). Finally, the matrix (M) protein inhibits host-cell antiviral mRNA export from the nucleus to the cytoplasm, thus inhibiting expression of key antiviral proteins, including interferons (IFN). Thus, mutation of the M protein generates a virus that is highly sensitive to IFN (Barber, 2005).

The oncolytic derivative of VSV, VSVΔ51, has a single amino acid deletion in its M protein at position 51, abrogating M protein function. This deletion restricts viral replication to cells with defective IFN signaling since an intact signaling pathway will result in abundant production of IFN and inhibit virus replication. A screen of the NCI60 panel of human cancer

cell lines revealed that 65-70% of the tested cell lines had defects in the IFN pathway and thus could harbour VSVΔ51 replication (Stojdl et al., 2003).

1.2.2- SMALL MOLECULE VIRAL SENSITIZERS FOR OV THERAPY

Results from clinical trials as well as *ex vivo* patient tumour cultures suggest there is substantial heterogeneity in tumour sensitivity to infection by oncolytic viruses. In order to overcome this intrinsic heterogeneous response, the use of small molecule enhancers of viral oncolysis has been explored. Among others, a category of small molecule viral sensitizers (VSes) have been specifically selected for their ability to overcome OV resistance in cancer cell lines using a high-throughput drug screen approach (Diallo et al., 2010). Some of these compounds, for example the synthetic molecule VSe1, were found to enhance OV spread up to 1000-fold with retained selectivity towards cancer cells. Studies in a VSVΔ51-resistant syngeneic murine colon tumour model further demonstrated that tumour progression could be delayed by treatment with VSVΔ51 in combination with VSe1 in comparison to monotherapies (Diallo et al., 2010).

Interestingly, many of the validated hits in the initial drug screen are described as microtubule destabilizing agents (MDAs). These are diverse small molecules of the colchicinoid, vinca alkaloid, and benzimidazole classes (described in section 4.1) and include drugs such as colchicine and vinorelbine which bind different sites on tubulin to destabilize microtubule structures (Jordan, 2002). More recent work has focused on elucidating how colchicine and other MDAs increase the oncolytic efficacy of VSVΔ51. Colchicine was found to inhibit the translation of a subset of proteins, and in particular that of type I IFNs. This led to improved spread of VSVΔ51 in cancer cells. Furthermore, colchicine increased the proportion of neighbouring uninfected cells with more than one nucleus (polynucleation) through the action of

secreted factors such as IL-8, IL-29, and IP-10 leading to bystander killing. Importantly, the combination between MDAs and oncolytic rhabdoviruses such as VSVΔ51 was shown to be effective in several xenograft, syngeneic, and transgenic models of cancer (Arulanandam et al., 2015).

The discovery of viral sensitizers has provided a novel means to improve OV spread in resistant cell lines. Furthermore the identification of MDAs as potent VSes provides a rationale for further probing of such combinations in OV therapy. This combination is particularly attractive since microtubule targeting agents (e.g. Vinorelbine) are still used as standard of care for some indications (e.g. lung cancer).

1.2.3- OV CLINICAL TRIAL OVERVIEW

Many clinical trials involving OVs have been conducted and completed and are reviewed in (Miest and Cattaneo, 2014; Pol et al., 2014). The most clinically advances candidate viruses include Phase III trials for Amgen's talimogene laherparepvec (T-VEC) a herpes simplex virus for melanoma (NCT00769704), and Reolysin, a reovirus for head and neck cancer (NCT01166542). SillaJen's Pexa-Vec, a vaccinia virus in currently in Phase IIb for hepatic cancer (NCT01387555) while an Adenovirus and Maraba MG1 virus combination is currently recruiting patients (NCT02285816). The results from these trials suggest that while some patients benefit from OV therapy most patients do not, highlighting the need to improve therapy through engineering or combination strategies. The paradigm of OVs causing curative viral oncolysis has been replaced by one where OVs can be used to break tumour tolerance and engage the immune system which can then be complemented by anti-tumour immunomodulating agents (Lichty et al., 2014; Melcher et al., 2011).

1.3- MICROTUBULES

1.3.1- MICROTUBULE STRUCTURE AND DYNAMICS

Microtubules (MTs) play a key role in many cellular processes including the maintenance of cellular architecture, the intracellular movement of vesicles and organelles, and chromosome segregation during mitosis (Risinger et al., 2009a). MTs are highly dynamic structures which constantly undergo lengthening and shortening processes in response to the cell's needs. They are composed of α- and β-tubulin heterodimers which polymerize in a head-to-tail manner and further associate to form cylindrical structures (Nogales, 2000). Pools of free tubulin heterodimers also exist in the cell and their addition or subsequent removal from MTs is tightly regulated (Parker et al., 2014). The two MT ends are not equivalent; the plus end is capped by β-tubulin subunits while the minus end is capped by α-tubulin subunits with the former being the more dynamic of the two ends. Addition of tubulin on the plus end occurs in a guanosine-5'-triphosphate (GTP)-dependent manner; the β-tubulin subunit is bound to GTP which undergoes an irreversible hydrolysis to guanosine-5'-diphosphate (GDP) and inorganic phosphate. The loss of GTP without addition of a tubulin subunit, or loss of GDP cap will result in rapid shortening of the MT, known as MT catastrophe, due to exposure of the relatively unstable MT core (Nogales, 2000). Conversely, MT rescue is described as the transition from MT shortening to a paused or growth state.

MT polymerization dynamics can be described by dynamic instability and treadmilling behaviours. Dynamic instability refers to the stochastic shortening and lengthening of MT ends and can be described by the rate of MT lengthening/ shortening, the rate of MT catastrophe, and the rate of MT rescue (Jordan and Wilson, 2004). The plus end of the MT is the more

dynamically unstable of the two ends. Treadmilling denotes net growth of the MT at one end and net loss at the other end with no net change in MT mass (Jordan and Wilson, 1998).

1.3.2- THE ROLE OF MICROTUBULES IN MITOSIS

The modulation of MT dynamics is crucial during mitosis as they mediate the correct attachment of chromosomes to the spindle during prometaphase, the alignment of chromosomes at the metaphase plate during metaphase, and the separation of sister chromatids in anaphase and telophase (Jordan and Wilson, 2004). During prometaphase, MTs leaving from each of the two spindle points must lengthen and contract to find and become attached to the kinetochore of chromosomes until each chromosome is attached to two MT fibers, one from each spindle. The presence of a single chromosome that is not properly bound will be sufficient to block the cell's transition to anaphase which is controlled by the anaphase promoting complex (APC). The APC is composed of an E3 ubiquitin ligase and its co-activator, cell division control protein 20 (CDC20), and cyclin B. CDC20 functions by targeting securin thus preventing the degradation of cohesin on sister chromatids, while cyclin B, a cyclin dependent kinase 1 (CDK1) co-factor, targets proteins for proteasomal degradation (London and Biggins, 2014). Inhibition of APC function is achieved through CDC20 inactivation by the mitotic checkpoint complex and an extended blocking period will cause the cell to undergo apoptosis (London and Biggins, 2014).

1.4- MICROTUBULE TARGETING AGENTS

Microtubule targeting agents (MTAs) disrupt MT dynamics, which compromise the cell's ability to undergo mitosis, are widely used chemotherapeutic agents. MTAs inhibit cellular proliferation by interfering with the rapid polymerization and depolymerization dynamics required for proper spindle function and segregation of chromosomes during mitosis (Jordan and Wilson, 2004). The inhibition of MT dynamics ultimately blocks cells in G2/M and the

sustained blockage of these cells will lead to apoptosis or mitotic catastrophe (Mukhtar et al., 2014). MTAs can broadly be classified into 3 groups determined by the drug's tubulin binding site: vinca-, colchicine-, or taxane-binding sites (Nogales, 2000). Of these groups, colchicine- and vinca-binding site compounds are functionally described as microtubule destabilizing agents (MDAs), while taxanes are described as microtubule stabilizing agents (MSAs). MDAs and MSAs effectively suppress MT dynamics at low drug concentrations resulting in mitotic arrest, initiation of apoptosis, and mitotic catastrophe (Risinger et al., 2009a). At 10 to 100-fold higher concentrations, MDAs inhibit tubulin polymerization causing MT destabilization, while MSAs promote tubulin polymerization leading to MT stabilization (Jordan and Wilson, 2004).

1.4.1- MICROTUBULE STABILIZING AGENTS

MSAs include compounds from the taxane family (paclitaxel, docetaxel) and bind to β-tubulin subunits on the inside surface of the MT (Dumontet and Jordan, 2010). These drugs are mainstays in the treatment of a variety of malignancies including breast and ovarian cancers. Taxanes have been successfully combined with a variety of chemotherapeutic agents including combination with platinum based compounds such as cisplatin, anthracyclines, and more recently, HER2-tergeted therapies in breast cancer as will be discussed in section 1.5.2 (Kampan et al., 2015; Schmidt, 2014).

1.4.2- MICROTUBULE DESTABILIZING AGENTS

1.4.2.1-COLCHICINE

Colchicine was first isolated form the meadow saffron *Colchicum autumnale* in 1820 and was the first described MDA (Pelletier P.J., 1820) . Colchicine is able to bind to free tubulin heterodimers in solution forming a stable complex distorting the dimer and preventing its

polymerization. It also binds to tubulin polymers at the junction between α- and β-tubulin heterodimers in proximity to the GTP-binding site on β-tubulin blocking contact between tubulin protofilaments, leading to depolymerization (Risinger et al., 2009a). In addition to its action on MTs, colchicine has been found to inhibit *de novo* blood vessel formation and destroy existing vessels in the tumour microenvironment (Lu et al., 2012). Colchicine is used clinically as an anti-inflammatory in the treatment of gout and Mediterranean fever, and has been shown recently to be beneficial in cardiovascular diseases including pericarditis (Slobodnick et al., 2015).

1.4.2.2-VINCA-SITE BINDING AGENTS

Vinca alkaloids were isolated from the periwinkle plant, *Catharanthus roseau* in the 1950s by Noble and Beer and were found to have MT destabilizing capabilities (Noble et al., 1958). Binding of vinca alkaloids occurs on residues 175-213 of β-tubulin in close proximity to the GTP-binding site at the MT's plus end (Nogales, 2000). Compounds such as vinblastine and vincristine were used as chemotherapeutics starting at the end of the 1950s. Since then, semi-synthetic and synthetic analogs such as vinorelbine, and vinflunine have been developed and are currently being used for the treatment of a variety of cancers including non-small cell lung cancer, testicular cancer, and lymphoma (Risinger et al., 2009a). Other vinca-site binding agents include maytansine isolated from the *Maytenus ovatus* plant which was shown *in vitro* to be 100- to 1000-fold more toxic in a panel of human cancer cells lines than vinca alkaloids (Issell and Crooke, 1978; Oroudjev et al., 2010). Maytansinoid binding to tubulin potently suppresses MT dynamics, arresting cells in G2/M and ultimately leading to their death by mitotic catastrophe (Lewis Phillips et al., 2008).

1.4.3- LIMITATIONS OF MTA CHEMOTHERAPY

The inherent toxicity of MTAs and resulting narrow safety window limits the use of many MTAs as chemotherapeutic agents. For example, colchicine's immunomodulatory properties at low doses have led to its use in the treatment of gout but toxicities at effective anti-tumour doses have halted its progress in the clinic, while maytansinoids have proven too toxic to administer as chemotherapeutics (Risinger et al., 2009b). Similarly, despite their wide use, paclitaxel and docetaxel are often associated with neuropathy which is dose-cumulative and restricts treatment regimens, especially in combination with platinum-based compounds (Dumontet and Jordan, 2010). Other side effects of MTAs include bone marrow damage, gastrointestinal paralysis caused by neurological toxicity against the autonomic nervous system, peripheral axonal neuropathy, and neutropenia (Dumontet and Jordan, 2010; Lu et al., 2012). Strategies aimed at overcoming systemic toxicities of MTAs, by synthesis of semi-synthetic and synthetic compounds, or through conjugating MDAs to antibodies against known tumour antigens (as described further below) have consequently been employed to improve the safety window of MTAs.

1.4.4- ANTIBODY-DRUG CONJUGATES

Antibody-drug conjugates (ADCs) are composed of a monoclonal antibody targeting a cancer selective antigen, a cytotoxic drug, and a linker region that joins the two components (Lopus, 2011). The monoclonal antibody portion of the conjugate allows for specific binding to tumour cells expressing or overexpressing a given tumour antigen, often a cell surface receptor. Upon receptor binding, the antibody is internalized through receptor-mediated endocytosis and is encapsulated in a lysosome for degradation (Flygare et al., 2013; Lopus, 2011). This

internalization allows the cytotoxic drug to be delivered directly inside the target cell, thus highly cytotoxic drugs can be conjugated with low systemic toxicity.

Approximately 30 ADCs are currently undergoing clinical trials with 2 ADCs approved by the Food and Drug Administration (FDA): brentuximab vedotin (Adcetris) for the treatment of Hodgkin's lymphoma (targeting CD30) and trastuzumab emtansine (Kadcyla) for the treatment of human epidermal growth factor receptor (HER)2 positive metastatic breast cancer (MBC). The cytotoxic payloads in both the above ADCs are MDAs; monomethylauristatin E (MMAE) and derivative of maytansine 1 (DM1), respectively (Lopus, 2011). MDAs are well suited to being used in ADCs as they retain their high potency upon antibody conjugation which is important as the delivery of the cytotoxic payload is limited by the number of antigen molecules bound by antibody on the cell surface (Lambert and Chari, 2014).

1.5- HER2 AS A TARGET FOR CANCER THERAPY

1.5.1- HER2 AND BREAST CANCER

HER2 (erbB2/neu) is a proto-oncogene on chromosome 17 first described in 1982 (Padhy et al., 1982). Rats developing chemically-induced neuroblastomas presented a 185kDa phosphoprotein in their sera, which was found to be responsible for the transformation. The amplification of this protein (HER2) was subsequently found in 20-30% of human breast cancers (Nahta, 2012; Tafe and Tsongalis, 2011). HER2 overexpression can result from an increase in gene copy numbers and/or increase in HER2 protein synthesis and is associated with a poor disease prognosis and increased risk of metastasis especially to the brain (Alameddine et al., 2013; Gutierrez and Schiff, 2011). The presence of HER2 at the cell surface of cancer cells as well its low level of expression in normal tissue are favourable to the safety window of HER2 targeted therapies (Zaczek et al., 2005).

1.5.1.1- HER2 RECEPTOR AND ACTIVATION

HER2 is a member of the human epithelial growth factor family of tyrosine kinase (TK) receptors which also includes HER1, 3, and 4. The structure of the HER family of receptors include an extracellular cysteine-enriched sequence, a transmembrane domain, and an intracellular tyrosine kinase catalytic domain containing tyrosine autophosphorylation sites (Alameddine et al., 2013). The extracellular domain is divided into four subdomains, termed I through IV, and the interaction of these subdomains will determine the open or closed conformation of the receptor. The closed conformation involves the interaction of subunit II with IV, while the interaction of I with III opens the receptor and exposes the dimerization domain (II) favouring ligand binding (Sliwkowski, 2003). HER2, which lacks key residues in the contact region of subunit IV, is perpetually in an open state and ready to partner (Sliwkowski, 2003).

EGFR family ligands include epidermal growth factor (EGF) and tumour growth factor-α (TGF-α) which preferentially bind to HER1 (EGFR) as well as neuregulins which preferentially bind to HER3 and HER4 (Alameddine et al., 2013) . Binding of ligand to the extracellular domain induces receptor dimerization and results in the activation of the intracellular TK domain which then autophosphorylates its tyrosines residues. The autophosphorylation of the tyrosine residues activates them and allows binding with proteins harbouring a Src homology 2 (SH2) domain initiating various signaling cascades (Alameddine et al., 2013). Tyrosine kinase inhibitors (TKIs) such as gefitinib block the binding of adenosine triphosphate (ATP) to the receptor's intracellular domain thus obstructing TK activity and downstream signaling (Press and Lenz, 2007).

Receptor dimerization is crucial for signal transduction and occurs in a heterodimeric fashion between HER family members. HER2 is unique in that does not bind to a ligand, thus its activation relies on heterodimerization with another HER member which is favoured by its natural open conformational state (Gutierrez and Schiff, 2011). Furthermore, HER2 has the strongest catalytic kinase activity and therefore the strongest signaling activity. Conversely, HER3 possesses a ligand binding domain with the highest affinity, but lacks an activating kinase domain (Alameddine et al., 2013).

1.5.1.2- PATHWAYS ACTIVATED BY HER2 SIGNALING

HER2-HER3 dimer formation is favoured and strongly activates the phosphoinositide 3-kinase/ protein kinase B/ mammalian target of rapamycin (PI3K/Akt/mTOR) pathway and also activates the mitogen-activated protein kinase/ extracellular signal-regulated kinase 1/2 (MAPK/ERK1/2) pathway via Ras. Activation of these pathways has many effects including inhibition of apoptosis, stimulation of angiogenesis, promoting cell proliferation and differentiation, and also increasing cancer invasion and metastasis (Gutierrez and Schiff, 2011; Nahta, 2012).

1.5.1.2.1- PI3K/AKT/mTOR

PI3Ks are heterodimeric lipid kinases composed of a p85 regulatory and p110 catalytic subunits (Cantley, 2002). PI3K activation upon growth factor stimulation allows it to phosphorylate the plasma membrane lipid phosphatidylinositol-4, 5-biphosphate (PIP_2) to phosphatidylinositol-3, 4, 5-triphosphate (PIP_3) which results in the membrane translocation of Akt. Phosphoinositide-dependent kinase-1 (PDK-1) then phosphorylates Akt, resulting in its activation (Cantley, 2002). Activation of Akt results in the inactivation of glycogen synthase kinase-3β (GSK3β) relieving the repression on potential oncogenic transcription factors Jun and

Myc (Zhao and Vogt, 2008). Furthermore, Akt activates mTOR increasing transcription through concerted action on ribosomal protein S6 kinase and eukaryotic initiation factor 4E binding protein (Paplomata and O'Regan, 2014). Akt activation also influences apoptosis through activation of NF-κB which upregulates pro-survival B-cell lymphoma extra-large (BCL-XL) as well as inhibiting anti-apoptotic genes such as Fas ligand (Zaczek et al., 2005). Hyperactivation of HER2 signaling also increases c-myc and cyclin D, impacting G1-S cell cycle transition. Increases in these proteins leads to the sequestration of p27, a cyclin-dependent kinase inhibitor responsible for the regulation of the cyclin E-CDK2 complex mediating cell cycle entry. Thus, increases in c-myc and cyclin D allow for cyclin E-CDK2 activity and increased cellular proliferation (Zaczek et al., 2005). Globally, activation of PI3K/Akt/mTOR increases cell replication and promotes cell survival while reducing apoptosis (Zhao and Vogt, 2008).

1.5.1.2.2- MAPK/ERK

MAPK/ERK1/2 pathway activation is mediated by growth factors whose binding to ligand result in the phosphorylation and activation of Ras which leads to phosphorylation of the ERK signal transducer and causes its nuclear shuttling (Reddy et al., 2003). ERK affects a number of transcription factors including activating protein-1 (AP-1) which can stimulate cell migration and angiogenesis by promoting the activity of matrix metalloproteinases. The transcription of carbamoyl phosphate synthetase II (CPS II) is also affected by ERK mediated AP-1 activation. CPS II leads to the stimulation cell cycle progression and inhibition of a cell's apoptotic response to stimuli including hypoxia, growth factor removal, and chemotherapeutic agents (Burotto et al., 2014; Reddy et al., 2003).

1.5.2- CHEMOTHERAPEUTIC AGENTS TARGETING HER2

1.5.2.1- TRASTUZUMAB

Trastuzumab was approved for the treatment of breast cancer in 1998 and is a humanized immunoglobulin G (IgG) monoclonal antibody targeting the extracellular subdomain IV of HER2 (Hudis, 2007; Tafe and Tsongalis, 2011). Trastuzumab works on several fronts. Binding of trastuzumab to the HER2 receptor prevents the activation of the receptor's intracellular TK and also decreases the presence of HER2 receptors at the cell surface, thus attenuating PI3K signaling (Bianchini and Gianni, 2014; Hudis, 2007). Second, antibody binding prevents the formation of p95, a constitutively active extracellular membrane-bound variant of HER2 (Arribas et al., 2011; Nahta, 2012). Finally, the fragment crystallisable (Fc) portion of trastuzumab can be recognized by natural killer cells which become activated, leading to antibody-dependent cell-mediated cytotoxicity (ADCC) of the HER2 overexpressing cell (Nahta, 2012). Thus, trastuzumab is able to both antagonise the anti-apoptotic and pro-growth signaling from the PI3K pathway and engage the host immune system via ADCC.

Clinically, trastuzumab has been shown to synergize with chemotherapeutic modalities including cisplatin, carboplatin and docetaxel and to have additive effects when combined with doxorubicin, cyclophosphamide, methotrexate, and paclitaxel (Slamon et al., 2001). These results are supported by phase III trial data where patients with MBC showed longer median time to disease progression and higher overall response in the chemotherapy plus trastuzumab group versus chemotherapy alone (Slamon et al., 2001). The trastuzumab and vinorelbine or taxane study, which compared trastuzumab plus either vinorelbine or a taxane further demonstrated an increase in progression free survival and no significant increase in adverse events with both combination treatments (Burstein et al., 2007). Finally, a meta-analysis of randomized trials combining trastuzumab with chemotherapeutics in a neoadjuvant setting concluded that the

addition of trastuzumab benefited patient responses and did not compromise patient health (Valachis et al., 2011). The observed clinical benefits of combining trastuzumab with chemotherapeutic modalities highlighted the potential of ADCs as a new tool for cancer treatment.

Despite the success of trastuzumab either alone, or in combination with standard chemotherapy approximately 75% of breast cancers do not respond to treatment (Chung et al., 2006; Kim et al., 2008). In addition to treatment non-responsive tumours, trastuzumab responsive tumours can acquire drug resistance. Resistance can be acquired by several mechanisms including epitope masking by membrane mucins, which reduce antibody binding to HER2, truncation of the HER2 receptor into the constitutively active non-trastuzumab binding p95 fragment, and hyperactivation of downstream signaling though PI3K (Nahta, 2012). The limited response rate and resistance mechanisms have spurred the development of other HER2 targeting monoclonal antibody therapies.

1.5.2.2- PERTUZUMAB

Pertuzumab is also a humanized monoclonal antibody targeting HER2. In contrast with trastuzumab, it binds to the extracellular domain II on HER2 (Scheuer et al., 2009). Unlike trastuzumab which negates HER2 activation, pertuzumab blocks the formation of HER2 containing dimers, including HER1-HER2 and HER3-HER2 complexes (Agus et al., 2002). This blockage decreases HER2 phosphorylation and reduced the activation of downstream MAPK and Akt. In addition to its activity on HER signaling, pertuzumab was found to inhibit cancer cell growth independent of HER2 expression levels (Agus et al., 2002). Thus, unlike trastuzumab, pertuzumab has activity in HER2 normal or low expressing cancer cell lines. The binding of pertuzumab and trastuzumab to separate epitopes on the extracellular domain of

HER2 led to the hypothesis that combination of the two antibodies could more potently suppress tumour growth. Indeed, in murine xenograft breast and non-small cell lung cancer models, combination of trastuzumab with pertuzumab enhanced anti-tumour activity (Scheuer et al., 2009).

The first phase I study showed that the pharmacokinetic properties of pertuzumab were similar to trastuzumab and included patients that did not show amplification of HER2 but had a response to the treatment (Agus et al., 2005). Phase II trials conducted with pertuzumab as a single-agent, or in combination with trastuzumab or other chemotherapeutics show modest effect with pertuzumab alone and increased efficacy in combination treatments (Jhaveri and Esteva, 2014). The approval of pertuzumab in 2012 by the US FDA for metastatic breast cancer was based on the positive results from the randomized, double-blind Clinical Evaluation of Pertuzumab and Trastuzumab Trial (CLEOPATRA) which evaluated the safety and efficacy of pertuzumab plus trastuzumab and docetaxel, compared to placebo plus trastuzumab and docetaxel. Improved median overall survival, progression-free survival, and duration of response was seen in the pertuzumab group compared to the control group (Swain et al., 2015).

1.5.2.3- TRASTUZUMAB EMTANSINE

Trastuzumab emtansine (T-DM1) is a HER2 targeting ADC composed of trastuzumab conjugated by thioether linkage to an average of 3.5 DM1 molecules per antibody (Peddi and Hurvitz, 2014). T-DM1 retains the monoclonal targeting activities of unconjugated trastuzumab but is equipped with DM1 as a potent MDA that is released upon uptake by HER2 overexpressing cells (Junttila et al., 2011; Nahta, 2012). The conjugation of maytansine to trastuzumab occurs on lysine residues of the antibody via a thioether linker 4-[N-maleimidomethyl]-cyclohexane-1-carbonyl (MCC) using an added thiol substituent on

maytansine (Lambert and Chari, 2014). The binding of trastuzumab to the HER2 receptor leads to receptor-mediated endocytosis of the ADC which undergoes proteolytic degradation in the lysosome releasing the active lysine-MCC-DM1 metabolite (Corrigan et al., 2014). In addition to the described effects on HER2 signaling, lysine-MCC-DM1 has a potent destabilizing effect on MT causing cell to arrest in G2/M.

Phase I dose escalation trials in MBC patients determined the maximum tolerated dose (MTD) to be 3.6mg/kg while reported adverse effects included low grade elevated hepatic transaminases, decreased left ventricular ejection fractions (LVEF) anemia, fatigue, and nausea (Hurvitz et al., 2013). Phase II trials TDM4450g and TH3RESA showed a significant increase in progression free survival (PFS) over trastuzumab plus docetaxel, and physician's choice treatment, respectively (Hurvitz et al., 2013; Krop et al., 2014; Perez et al., 2014). The phase III EMILIA trial comparing T-DM1 with capecitabine plus lapatinib registered significant PFS and less adverse effects in the T-DM1 treatment arm (Verma et al., 2012; Welslau et al., 2014). This led to its approval by the FDA in February 2013 for MBC in patients who had previously received single or combination treatment with trastuzumab and/or a taxane and who developed disease recurrence during treatment or up to 6 months thereafter (Corrigan et al., 2014).

1.6- RATIONALE

HER2 targeting monoclonal antibodies have come to establish themselves as mainstays of HER2 positive breast cancers and gastric cancers and are under evaluation for other malignancies including non-small-cell lung cancer (Dreanic et al., 2015; Lara et al., 2004). Although there has been success in improving overall survival and time to disease progression, low drug response rates and acquired drug resistance remain hurdles to long-term survival (Alameddine et al., 2013; Barok et al., 2014). Furthermore, acquired HER2 overexpression has

not been shown to correlate with response to trastuzumab therapy (Chung et al., 2006; Kim et al., 2008). The combination of HER2 antibodies with chemotherapeutic agents is yielding better results, showing the promise for combination therapies with antibodies.

OVs are multi-modal anti-cancer agents which have made important strides in clinical trials with several clinical candidates and FDA approval pending on T-VEC (Amgen). Despite some success, tumour heterogeneity and response to OVs still remains an obstacle to single agent OV therapy (see section 1.2.3). In order to overcome such limitations, combination therapies with OVs are being explored to increase therapeutic benefit. OVs are a flexible platform that can be combined with a variety of existing therapies, including antibodies and chemotherapeutic agents, to improve efficacy (Fillat et al., 2014; Harrington et al., 2010; Jiang et al., 2015).

Although many combination therapies with OVs have been pursued, the use of cancer-targeted monoclonal antibodies with VSVΔ51 has thus far remained poorly explored. We hypothesized that the mechanisms leading to treatment resistance to anti-HER2 antibodies are likely different to those arising from OV therapy, suggesting these may be complementary treatment modalities. We further hypothesized that co-treatment with VSVΔ51 and trastuzumab, pertuzumab, or T-DM1 could lead to improved anti-cancer efficacy.

2-MATERIALS AND METHODS

2.1-CELL LINES

786-0 (human renal carcinoma), GM38 (primary human fibroblasts), SK-OV3 (human ovarian adenocarcinoma), JIMT-1 (human herceptin-resistant breast cancer), BT549 (human mammary epithelial), HS 578T (human mammary epithelial), T47D (human mammary epithelial), MDA-MB-231 (human mammary metastasis), and Vero (African Green Monkey kidney, CCL-81) were maintained in Dulbecco's modified Eagle's medium (DMEM; HyClone) + 10% fetal bovine serum (FBS; Gibco). SK-OV3, OVCAR8 (human ovarian), MCF-7 (human mammary adenocarcinoma), AF2068 (primary patient ascites sample), and OVCA 433 (human ovarian carcinoma) cells were maintained in Roswell Park Memorial Institute medium (RPMI; ATCC) + 10% FBS. OVCA 433 cells were a generous gift from Dr. Barbara Vanderhyden. JIMT-1 (ACC589) cells were obtained from the Leibniz Institute DSMZ-German Collection of Microorganisms. 786-0, GM38, SK-OV3, BT549, HS 578T, T47D, MDA-MB-231, OVCAR8, MCF-7, and Vero cells were obtained from the American Type Culture Collection. All cells were incubated at 37 °C in a 5% CO_2 humidified incubator.

2.2-VIRUSES

The oncolytic versions of Vesicular stomatitis virus encoding a firefly luciferase protein tag (VSVΔ51-Fluc) or encoding a green fluorescent protein (VSVΔ51-GFP) tag were grown and titered on Vero cells. Viruses were subsequently purified by 0.22 µm filtration and by Optiprep (Sigma) gradient (Diallo et al., 2012). For all virus infections, viruses were diluted in serum free DMEM to obtain the specified multiplicity of infection (MOI), or for mock infection conditions cells were supplemented with the same volume of serum free DMEM.

2.3-DRUGS AND ANTIBODIES

Herceptin (trastuzumab; Roche) and Kadcyla (trastuzumab emtansine; Roche), and Perjeta (pertuzumab; Roche) were obtained from clinical preparations and stored at 4 °C. Iressa (gefitinib; Cayman chemicals) was resuspended in 100% DMSO to 25 mM and was stored at -20 °C. Recombinant human NRG1-β1/HRG1- β1 EGF domain (R&D Systems) was resuspended in sterile PBS with 0.1% BSA and stored at -20 °C, recombinant human (TGF-α) (R&D Systems) was reconstituted in sterile 10 mM acetic acid and stored at -20 °C. Colchicine was obtained from Sigma and a stock of 100 mM was prepared in 100% DMSO and stored at -80 °C. Drugs were diluted to specified condition in serum free media for all assays.

2.4-DOSE RESPONSE CURVES

786-0 or GM38 cells were plated at a density of 30,000 cells/well in 96 well plates and incubated overnight at 37 °C in a 5% CO_2 humidified incubator. Cells were then treated with specified drug concentrations and infected 4h later with VSVΔ51-Fluc or VSVΔ51-GFP (MOI 0.1, 0.01, or 0.001) or mock infected. Cellular metabolic activity was assessed by AlamarBlue® (resazurin; BioRad); 10% of the total well volume of dye was added to each well. Following a 2h incubation, fluorescence emission was assessed at 450 nm as per manufacturer's protocol (Fluoroskan Ascent, Thermo Fisher). Samples were frozen and titered by standard plaque assay (VSVΔ51-GFP) (Diallo et al., 2012) or using a high-throughput titration method (VSVΔ51-Fluc) (see appendix 1(Garcia et al., 2014)).

2.5-IFNβ ELISA

786-0 cells were plated at a density of 250,000 cells/well in 12 well plates and incubated overnight 37 °C in a 5% CO_2 humidified incubator. Cells were then treated with specified drug

concentrations and infected 4h later with VSVΔ51-GFP at an MOI of 0.1 or mock infected. Twenty hours post-infection, cell supernatant was collected and frozen with 1:100 protease inhibitor complex (Roche). Verikine human IFNβ ELISA (PBL Interferon Source) kits were used following the manufacturer's instructions and IFNβ values (pg/ml) were interpolated from the obtained standard curve.

2.6-CELL LYSIS AND WESTERN BLOTTING

Whole cell lysates were obtained by lysing the cells in 50mM Hepes, pH 7.4, 150nM NaCl, 2mM Na_3VO_4, 10mM EDTA, 100mM NaF, 10mM $Na_2P_20_7$, protease inhibitor cocktail (Roche) and 1% Triton X-100. Protein concentration was determined by Bradford assay (BioRad) and 10-20ug of cell extract were run using the NuPAGE SDS-PAGE system (Invitrogen) and transferred onto a nitrocellulose membrane (BioRad). Membranes were blocked with 5% milk in TBS-T and probed with a rabbit polyclonal antibody to β-actin (Cell signaling, 49705) as a loading controls, or a mouse monoclonal antibody to HER-2/ErbB2 (Thermo, Ma5-13105) followed by of horseradish-peroxidase conjugates rabbit or mouse secondary antibodies, respectively (Jackson ImmunoResearch Laboratory). Supersignal West Pico Chemiluminescent substrate (Thermo Scientific) was used to visualize the protein bands.

2.7-IMMUNOFLUORESCENCE

786-0 or GM38 cells were plated on sterile glass coverslips at a density of 50,000 or 100,000 cells/well in 12 well plates and incubated overnight 37 °C in a 5% CO_2 humidified incubator. Cells were then treated at the specified drug concentrations and infected 4h later with VSVΔ51-GFP at an MOI of 0.01 or mock infected. Twenty four hours post-infection, cells were permeabilized with 0.1% Triton-X 100, fixed with 4% paraformaldehyde and incubated

overnight at 4 °C in a humidified chamber with a goat α-β tubulin primary antibody (Invitrogen) diluted 1:400 in 1% bovine serum albumin (BSA). Following washes, coverslips were incubated for 1h at room temperature with a secondary donkey α goat Alexa 594 (Invitrogen) diluted 1:200 in 1% BSA. Coverslips were mounted on slides with ProLong Gold Antifade reagent with DAPI (Life technologies) and stored at 4 °C. Images were taken using the AxioCam HRm camera (Carl Zeiss Ltd, Toronto ON) mounted on the Zeiss Imager M1 microscope at . Polynuclear and infected cells were manually counted from 6 fields per experimental condition, in triplicate at 40X with a minimum of 100 cells counted per condition.

2.8-VSVΔ51 SCREEN, HER2 WESTERN BLOTTING, AND EGFR/HER2 TARGETING DRUG SCREEN

786-0, BT549, HS 578T, T47D, MDA-MB-231, OVCAR8, OVCA433, JIMT-1, SK-OV3, and MCF-7 cells were plated at a density of 30,000 cells/well in 96 well plates and incubated overnight 37 °C in a 5% CO_2 humidified incubator. Cells were infected the next day with VSVΔ51-GFP or VSVΔ51-Fluc at MOIs of 1, 0.1, 0.01, 0.005, 0.001, or mock infected. GFP pictures of VSVΔ51-GFP infected plates were taken 24 and 48h post-infection. Cellular metabolic activity was assessed by AlamarBlue® (resazurin; BioRad); 10% of the total well volume of dye was added to each well. Following a 2h incubation, fluorescence emission was assessed at 450nm (Fluoroskan Ascent, Thermo Fisher). Samples infected with VSVΔ51-Fluc were frozen and subsequently titered using a high-throughput titration method (Garcia et al., 2014). Cells were also seeded at a density of 300,000 cells/well in 6 well plates, lysed 48h later, and subsequently blotted for HER2 as previously described.

For the drug screen, cell lines were plated at the above density and pre-treated for 4h with indicated doses of erlotinib, gefitinib, herceptin, pertuzumab, recombinant human neuregulin-β1,

recombinant human TGF-α, and EGF and infected with VSVΔ51-Fluc at MOI 0.1. Cellular metabolic activity was assessed by AlamarBlue® (resazurin; BioRad); 10% of the total well volume of dye was added to each well. Following a 2h incubation, fluorescence emission was assessed at 450nm (Fluoroskan Ascent, Thermo Fisher). Samples infected with VSVΔ51-Fluc were frozen and subsequently titered using a high-throughput titration method (Garcia et al., 2014).

2.9- IFNβ PRODUCTION AND RESPONSE ASSAYS

786-0, BT549, HS 578T, T47D, MDA-MB-231, OVCAR8, OVCA433, JIMT-1, SK-OV3, and MCF-7 cells were plated at a density of 30,000 cells/well in 96 well plates or at 300,000 cells/well in 12 well plates and incubated overnight 37 °C in a 5% CO_2 humidified incubator. An IFNβ ELISA was used to assess the production of IFNβ from the supernatant of cells which were infected with VSVΔ51-GFP at an MOI of 0.1 for 20h. Response to IFN was determined by pre-treating cells with IFNα (IntronA, Merck) or IFNβ (R&D Systems) for 2h prior to infecting with VSVΔ51-GFP at MOIs of 0.1 and 0.01.

2.10-EX VIVO SAMPLE PROCEDURE

SK-OV3 cells (5E6) were implanted subcutaneously into CD1 nude mice (Charles River Laboratories, Waltham MA)). When tumours reached 10mm x10mm, mice were culled and the tumours removed. Tumours were then sectioned and cored using a 2mm biopsy punch (Miltex) (Diallo et al., 2011). Following this procedure, cores were treated with Kadcyla, Herceptin, colchicine or mock treated at indicated doses and infected with 3E4 pfu VSVΔ51-GFP two hours post-treatment, or mock infected. GFP pictures were taken 24 and 28h post-infection. Cores and supernatants were collected and homogenized (Tissue Lyser, QIAGEN) at a later time point and subsequently titered by standard plaque assay as described above.

2.11-SK-OV3 NUDE MOUSE MODEL

Female CD-1 nude mice (Charles River Laboratories, Waltham MA) were implanted subcutaneously with 1E7 SK-OV3 cells suspended in 100ul PBS. When tumours reached 5mmx5mm, mice were treated with PBS i.v or VSVΔ51-Fluc (1E8 pfu) i.t. on days 12 and 19. *In vivo* imaging was done on days 13 and 14 by in vitro imaging system (IVIS) (Perkin Elmer, Waltham, MA). Mice were injected i.p. with 200ul of 10mg/ml D-luciferin (Biotium) and temporarily anesthetized 5 minutes later with 3% isofluorane for imaging. Living Image (Perkin Elmer, Waltham, MA) was used to quantify IVIS signal. Tumours were measured every other day using an electronic caliper and volumes were calculated as (length x width^2)/2. Mice were culled when tumour volume reached 160mm^3 and in accordance with institutional guidelines review board for animal care (University of Ottawa ethical board, protocol OGHRI-58)

2.12- STATISTICAL ANALYSES

All graphs and statistical analyses were performed using GraphPad Prism v.6. Means of two groups were compared using two-tailed unpaired Student's t-test. Means of more than two groups were compared by one-way ANOVA with Dunnett's multiple correction test. Two-way ANOVA with Dunnett's multiple correction test was applied when groups were split on two independent variables.

3-RESULTS

3.1- RELATIONSHIP BETWEEN HER2 EXPRESSION AND VSVΔ51 SENSITIVITY IN A PANEL OF CANCER CELLS

3.1.1-HIGH HER2 EXPRESSION IS ASSOCIATED WITH INCREASED VSVΔ51 OUTPUT BUT NOT WITH IFNβ SECRETION

We initially set out with the hypothesis that the mechanisms of resistance to HER2 targeting antibodies and VSVΔ51 are likely different given these modalities target different cancer-associated phenotypes; respectively EGFR hyper-activation and defective IFN signaling. As a first approach to test this hypothesis, we screened for VSVΔ51 sensitivity and HER2 expression in a small panel of ten cancer cell lines of various tissue origins including breast, ovary, and kidney.

A range of susceptibility to VSVΔ51 was found within the tested cell lines with VSVΔ51 output (titer) varying over 1000-fold from the most resistant (~1E4 pfu) to the most sensitive (~1E7 pfu) cell lines (**Figure 1a**). As with viral output, there was a range in the baseline levels of HER2 expression within the cell lines (**Figure 2a**). Cell lines such as SK-OV3 and JIMT-1 overexpressed HER2 by western blotting, while HER2 was not detectable in BT549 and HS 578T lines, with the rest of the cell lines having low HER2 expression. Based on HER2 expression, these ten cell lines were grouped into HER2-high and HER2-low cell lines and virus output between these groups was analysed (**Figure 2b**). Interestingly, cell lines with HER2 expression above the median were found to produce significantly more virus upon VSVΔ51 infection relative to their HER2-low counterparts. This screen suggested that HER2 overexpressing cell lines produce more virus.

a

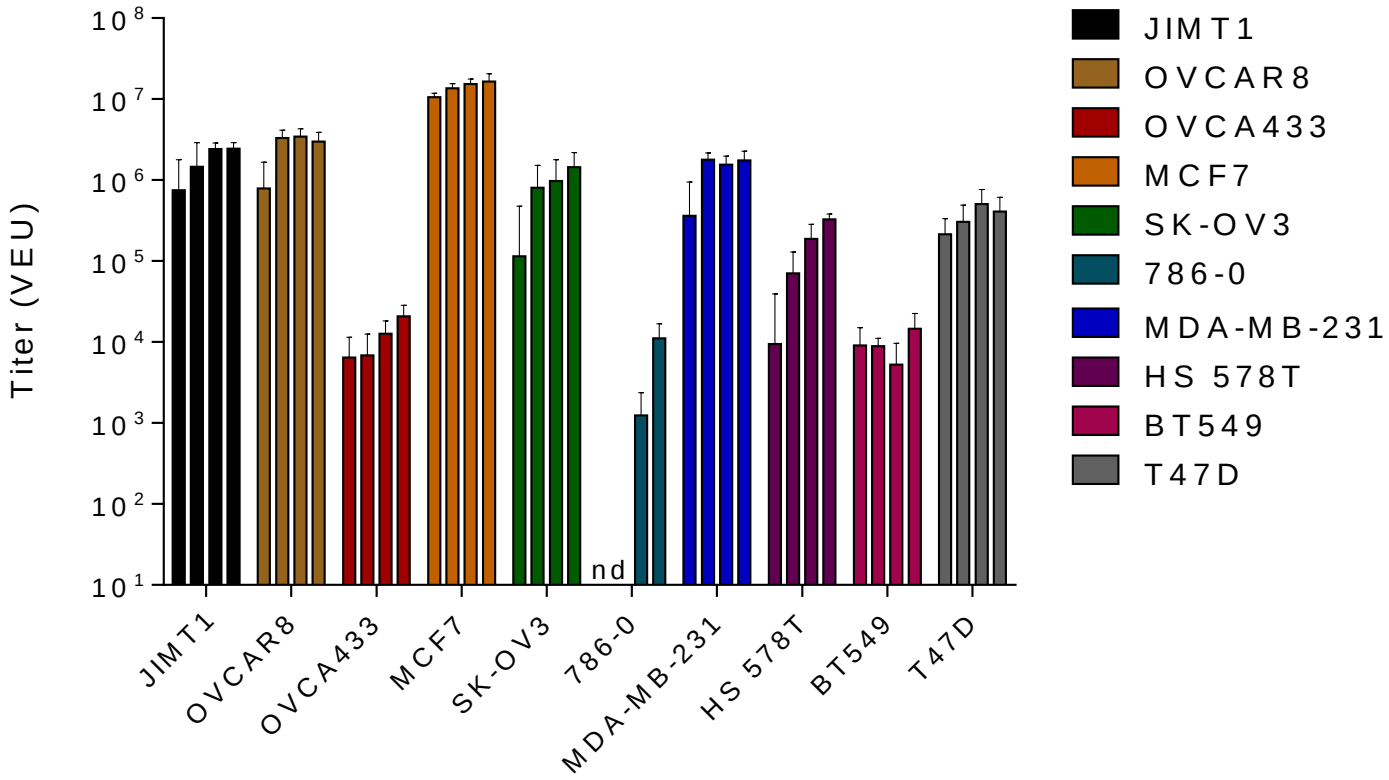
Titer (VEU)
10 8
10 7
10 6
10 5
10 4
10 3
10 2
10 1
nd
JIMT1
OVCAR8
OVCA433
MCF7
SK-OV3
786-0
MDA-MB-231
HS 578T
BT549
T47D

b

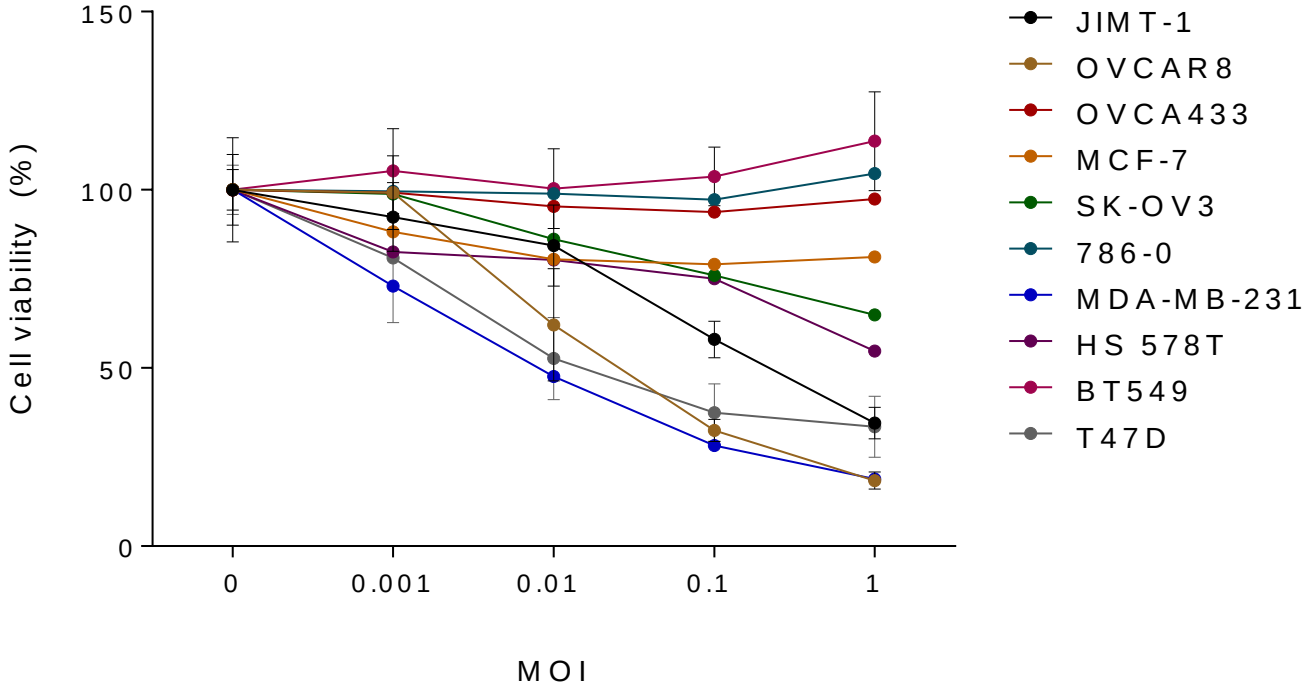
Cell viability (%)
150
100
50
0
0
0.001
0.01
0.1
1
MOI
JIMT-1
OVCAR8
OVCA433
MCF-7
SK-OV3
786-0
MDA-MB-231
HS 578T
BT549
T47D

Figure 1. Screen of a panel of 10 cell lines revealed differences in VSVΔ51 cytotoxicity and replication. (a) Cell lines were infected with VSVΔ51-Fluc at MOIs 0.001, 0.01, 0.1,1 (from left to right on histogram) or mock infected and titered 48h post-infection point using a high-throughput titration method. **(b)** Cell viability was assessed by Alamar Blue 48h post-infection. Data represent the average of 10 experimental replicates ± SD.

a

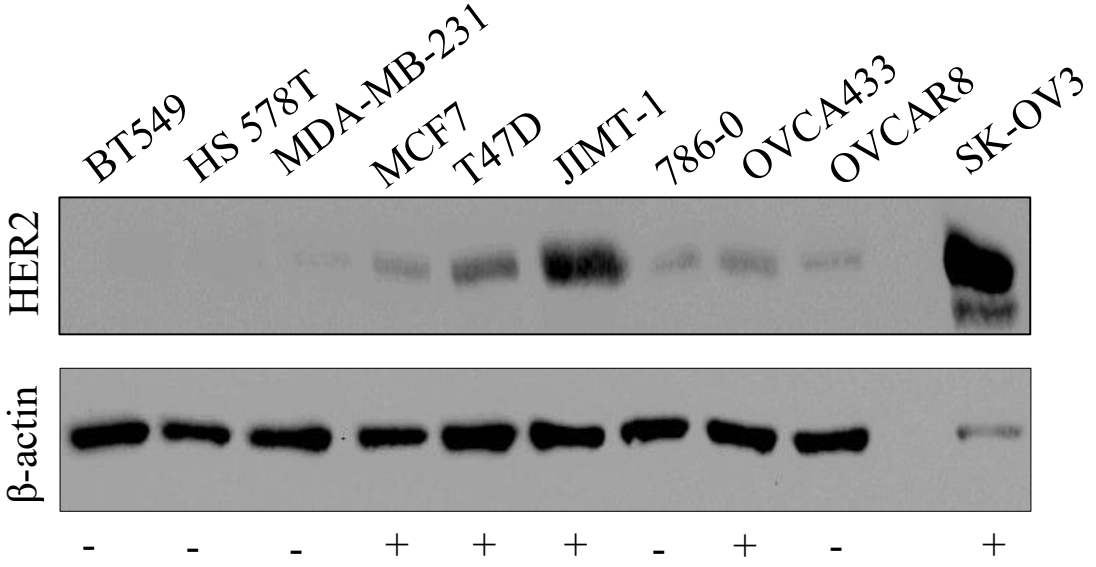
BT549
HS 578T
MDA-MB-231
MCF7
T47D
JIMT-1
786-0
OVCA433
OVCAR8
SK-OV3
HER2
β-actin
- - - + + + - + - +

b

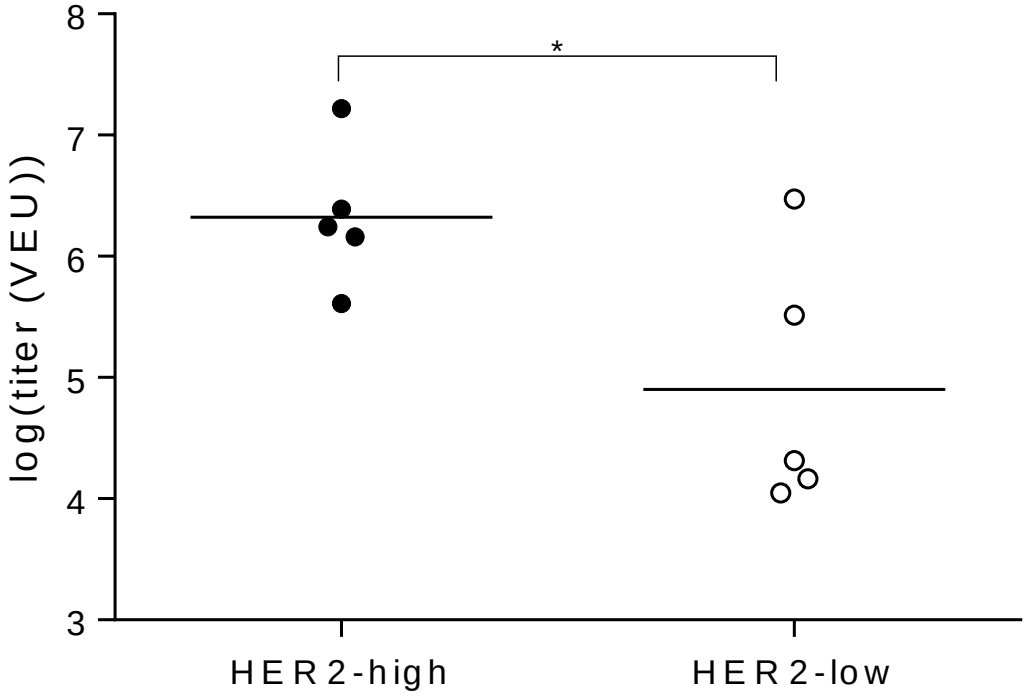
8
7
6
5
4
3
log(titer (VEU))
*
HER2-high
HER2-low

Figure 2. HER2-high expression is associated with an increase in VSVΔ51 output. (a) Western blot showing HER2 (top) and β-actin (bottom) expression levels from cell lysates of the tested cell lines. HER2-high cell lines are designated by "+" and HER2-low by "-". **(b)** The above cell lines were sorted into HER2-high and HER2-low expression based on protein levels. The viral output following infection with VSVΔ51-Fluc at MOIs 1 of the two groups was compared (VEU from figure 1a). Cell lines with baseline expression above the median produce significantly more virus (*p> 0.05; Fisher's exact test).

The capacity of the cell lines to produce and respond to IFN was also assessed as this could be an influencing factor on virus output following infection. First, all cell lines were pre-treated with either human IFNα or IFNβ followed by infection with VSVΔ51 to qualitatively measure the cell lines' ability to respond to exogenous IFN (**Figure 3a**). All cell lines were able to respond to exogenous IFN as shown by decreased VSVΔ51-GFP transgene expression (albeit viral growth was not fully blocked in MCF-7). IFNβ production following virus infection was assessed by ELISA (**Figure 3b**). Despite the relatively uniform response to exogenous IFN stimulation, secretion of IFNβ was found to be highly variable between cell lines. T47D, MCF7, and 786-0 cells could robustly secrete IFNβ in response to virus, whereas HS 578T, OVCAR8, and MDA-MB-231 cells produced very little IFNβ when stimulated by virus. Interestingly, there was no association between virus output and IFNβ secretion (**Figure 3c**); a cell line such as MCF7, for example, is highly permissive to VSVΔ51 replication (**Figure 1b**) despite its robust secretion of IFNβ, whereas OVCAR8 cells are also permissive to virus and are not able to secrete substantial amounts of IFNβ. Similarly, there was no statistically significant difference between HER2-high and –low cell lines with respect to their ability to secrete IFNβ.

a

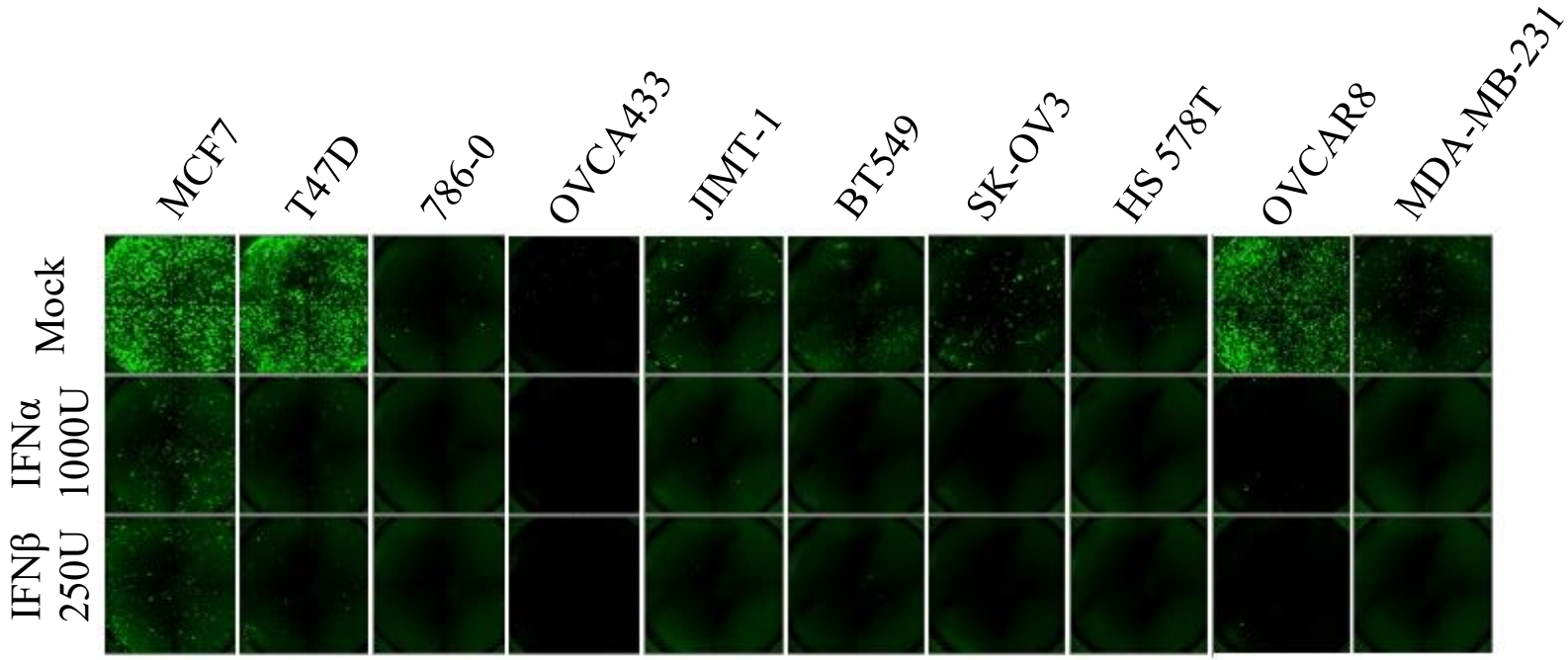
MCF7
T47D
786-0
OVCA433
JIMT-1
BT549
SK-OV3
HS 578T
OVCAR8
MDA-MB-231
Mock
IFNα 1000U
IFNβ 250U

b

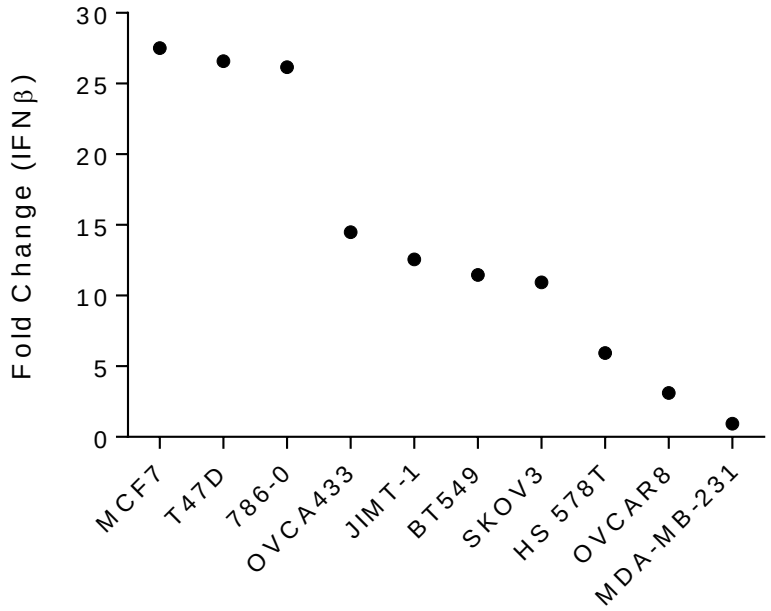
Fold Change (IFNβ)
30
25
20
15
10
5
0
MCF7
T47D
786-0
OVCA433
JIMT-1
BT549
SKOV3
HS 578T
OVCAR8
MDA-MB-231

c

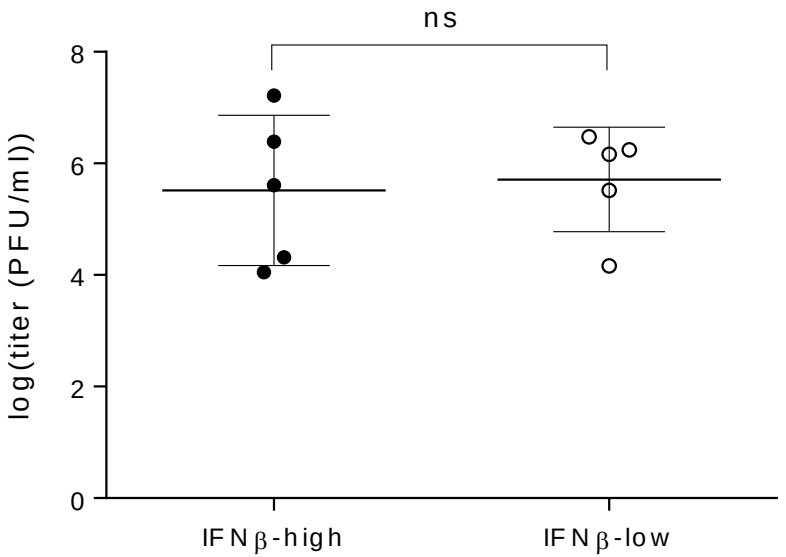
ns
log(titer (PFU/ml))
8
6
4
2
0
IFNβ-high
IFNβ-low

Figure 3. IFNβ-high expression is not associated with an increase in VSVΔ51 output. (a) Representative GFP pictures of cell lines pre-treated for 2h with IFNα (1000 IU or IFNβ 250 IU) and infected with VSVΔ51-GFP at MOI 0.1. Pictures were taken 24h post-infection. **(b**) Fold change in IFNβ secretion as measured by ELISA. Cell lines were infected with VSVΔ51 at MOI 0.1 and supernatants were collected 20h post-infection. **(c)** Cell lines were sorted into IFNβ-high and IFNβ-low expression based ELISA from (b). The mean virus titers between the two groups was compared; ns= not significant, Fisher's exact test.

3.1.2- VSVΔ51 CAN CURE HER2-HIGH TUMOUR XENOGRAFTS

Overall, the screening of a panel of cell lines revealed that HER2 overexpressing cells exhibited greater sensitivity to VSVΔ51. We wondered whether this could translate to efficacy of VSVΔ51 treatment in HER2 high tumours using an *in vivo* model of ovarian cancer in immunodeficient mice. The HER2-high SK-OV3 human cell line was chosen to assess the efficacy of VSVΔ51 as a single-agent (**Figure 4**). SK-OV3 xenografts were implanted subcutaneously in nude mice and 1E8 pfu of VSVΔ51-Fluc were administered twice with doses given one week apart (**Figure 4a**). Mice were imaged following the first virus treatment and low levels of virus could be detected up to 48h post-infection (**Figure 4b**). Mouse weights were tracked following both doses of virus and no significant weight loss was associated with intratumoural injection of virus (**Figure 4c**). Treatment of mice with VSVΔ51-Fluc led to a decrease in tumour volume compared to PBS treated animals (**Figure 4d**). Despite the low detection of transgene expression in the tumours of the mice, all mice treated with VSVΔ51 were cured of their HER2 overexpressing tumours while no such cures were observed in the PBS treated animals (**Figure 4e**).

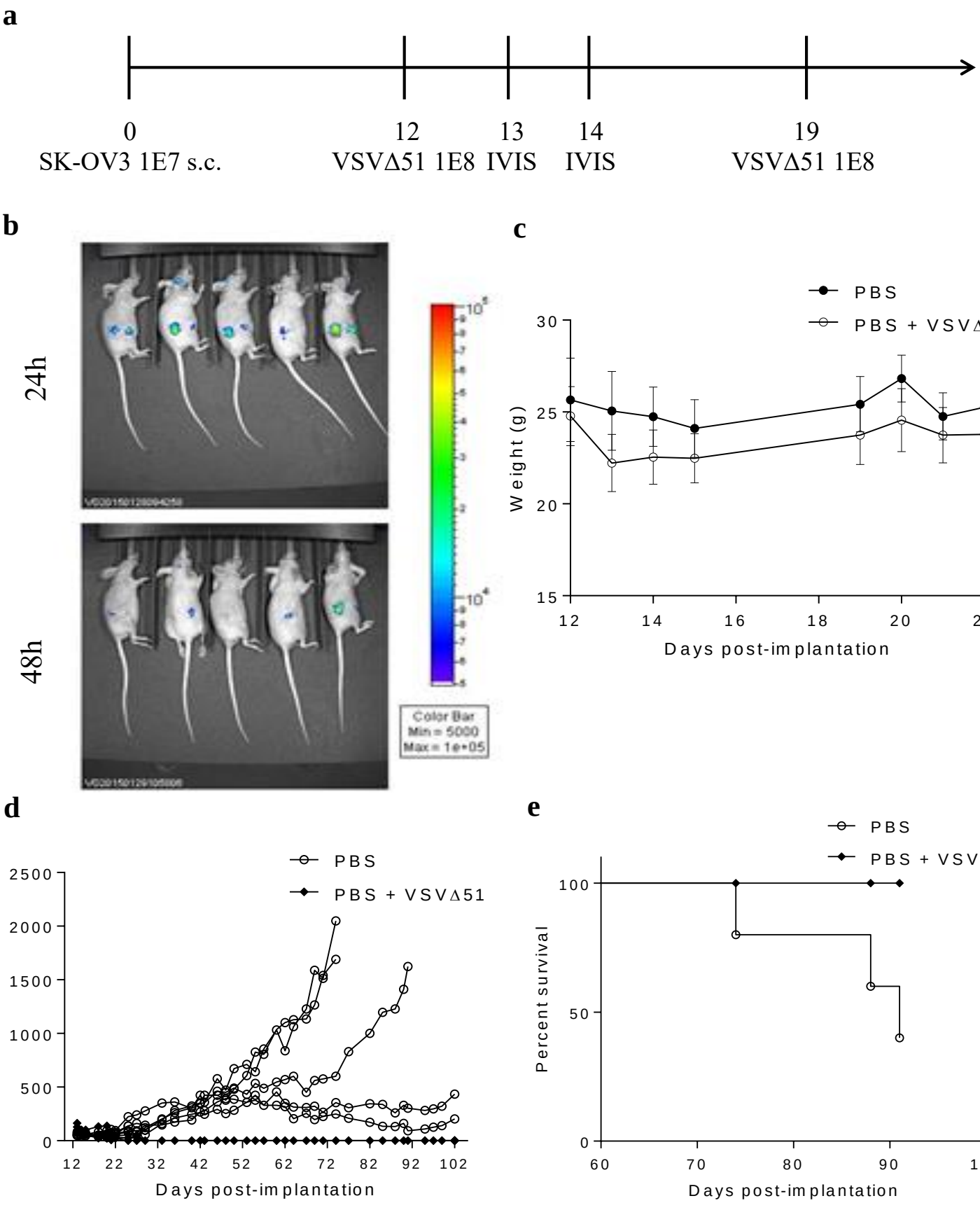
a
0
SK-OV3 1E7 s.c.
12
VSVΔ51 1E8
13
IVIS
14
IVIS
19
VSVΔ51 1E8
b
24h
48h
Color Bar
Min = 5000
Max = 1e+05
c
PBS
PBS + VSVΔ51
Weight (g)
Days post-implantation
d
PBS
PBS + VSVΔ51
Tumour volume (mm3)
Days post-implantation
e
PBS
PBS + VSVΔ51
Percent survival
Days post-implantation

Figure 4. HER2 overexpressing SK-OV3 xenografts can be cured by VSVΔ51 alone. (a) Experimental outline, 1e7 SK-OV3 cells were implanted subcutaneously on day 0. Mice received 1e8 pfu VSVΔ51-Fluc or PBS on days 12 and 19, with IVIS imaging on days 13 and 14. Tumours were measured until mice reached end point. **(b)** IVIS images 24 and 48h post-infection with VSVΔ51-Fluc. **(c)** Animal weights following treatment on days 12 and 19 **(d)** tumour volumes **(e)** Kaplan-Meier survival curve of the PBS and VSVΔ51-Fluc treated tumour bearing CD-1 nude mice, n=5 mice per group.

3.2- MODULATING EGFR PATHWAY INFLUENCES VSVΔ51 GROWTH

3.2.1- IMPACT OF EGFR FAMILY LIGANDS ON VSVΔ51 SPREAD

Given the association between HER2 and virus output, the data presented above suggested a role for EGFR activation in promoting VSVΔ51 growth. To examine the possibility that EGFR activation could modulate VSVΔ51 spread, we evaluated the impact of EGFR family activators, namely EGF, TGF-α, and Neuregulin-β1. EGF and TGF-α preferentially bind to and activate the EGFR whereas Neuregulin-β1 binding occurs preferentially on HER3 and HER4 receptors (Alameddine et al., 2013). Based on the positive association observed between HER2 and VSVΔ51, we expected that EGFR family activators should enhance VSVΔ51 growth, particularly in cell lines normally refractory to VSVΔ51. Indeed, we found that the majority of cell lines were rendered sensitive to VSVΔ51 by treatment with EGFR family receptor ligands, albeit to varying extents (**Figure 5**). These data suggest that signaling through EGFR family receptors affects VSVΔ51 growth.

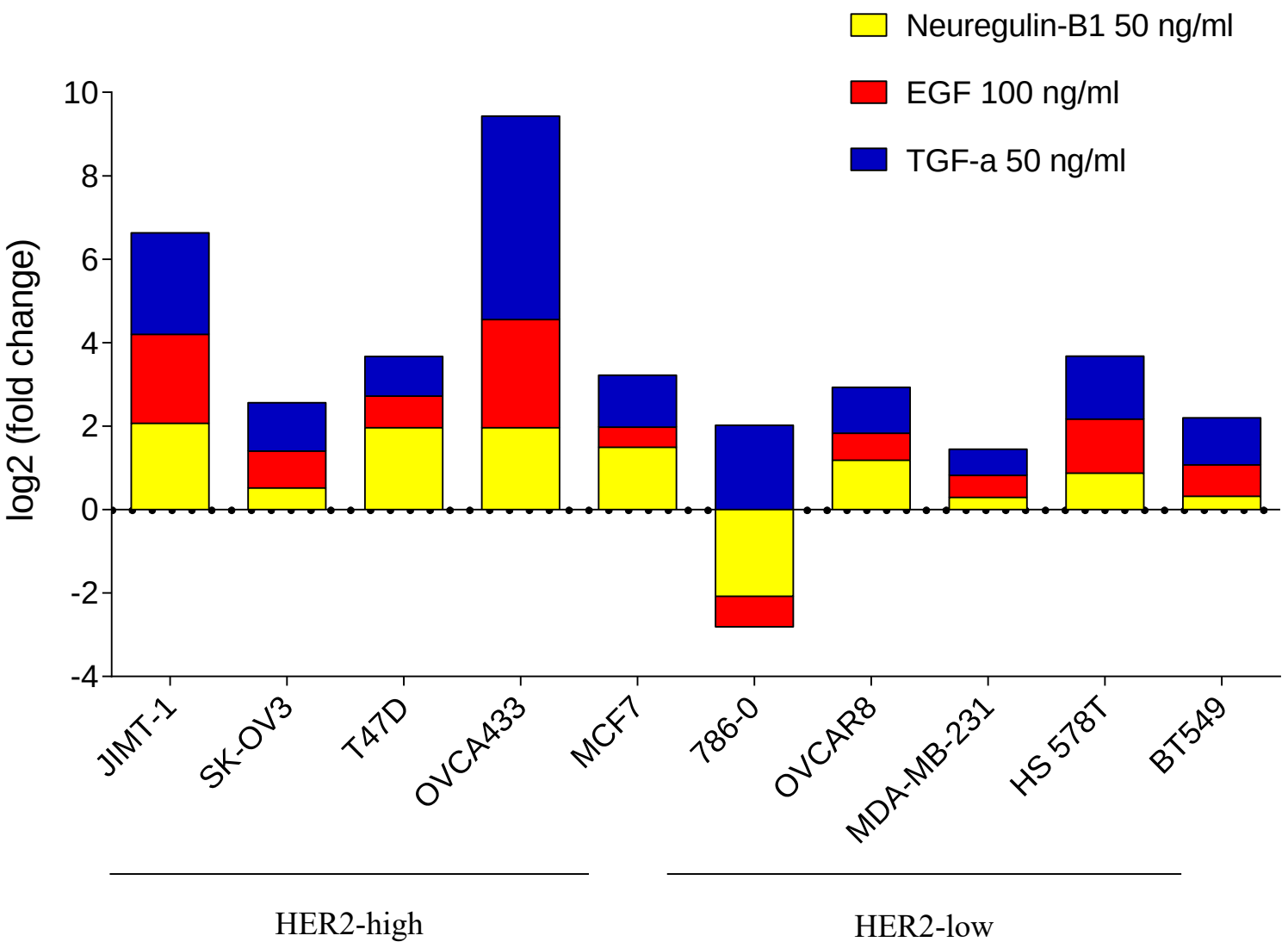
Neuregulin-B1 50 ng/ml
EGF 100 ng/ml
TGF-a 50 ng/ml
log2 (fold change)
10
8
6
4
2
0
-2
-4
JIMT-1
SK-OV3
T47D
OVCA433
MCF7
786-0
OVCAR8
MDA-MB-231
HS 578T
BT549
HER2-high
HER2-low

Figure 5. EGFR ligands promote virus spreading. Cell lines were pre-treated with, TGF-α 50mg/ml, EGF 100 ng/ml, or Neuregulin-β1 50ng/ml for 4h and infected with VSVΔ51-Fluc at MOI 0.1. Supernatants were titered 48h post-infection using a high-throughput method. Data represent the average of 3 experimental replicates ± SD.

3.2.2- IMPACT OF EGFR FAMILY RECEPTOR INHIBITION ON VSVΔ51 SPREAD

3.2.2.1- TRASTUZUMAB ANTAGONIZES VSVΔ51 SPREAD

Given that activators of EGFR family receptor ligands such as EGF and TGF-α and Neuregulin-β1 enhanced VSVΔ51 growth in most cell lines, we examined whether inhibiting the pathway using antibodies targeting HER2 could also impact viral growth. The combination of trastuzumab and VSVΔ51 was initially assessed in 786-0 cells, which express low levels of HER2 and are resistant to trastuzumab and also to VSVΔ51 infection *in vitro* (**Figure 6**). In the context of an *in vitro* infection, we found that trastuzumab significantly decreased VSVΔ51 titers in a dose dependent manner (**Figure 6a**) though neither the antibody alone nor the combination treatment exhibited cytotoxic effects (**Figure 6c**). Since 786-0 cells have a low baseline HER2 expression level, we further examined HER2 over-expressing SK-OV3 cells (see **Figure 2b**). In this context, high dose trastuzumab was also able to significantly decreased viral titers at a dose of 1000 µg/ml, which was the highest dose tested *in vitro* (**Figure 6b**). Further experiments revealed that this antiviral/inhibitory effect is also evident in an *ex vivo* context. Indeed, when tumour cores from SK-OV3 xenografts were pre-treated with trastuzumab and later infected with VSVΔ51-GFP there was a clear reduction in GFP transgene expression (**Figure 6d**). Furthermore, when the virus output from the cores and corresponding supernatants was titered through plaque assay, there was a significant decrease in pfu/ml relative to untreated controls (**Figure 6e**).

3.2.2.2- TRASTUZUMAB, PERTUZUMAB, AND GEFITINIB ELICIT AN ANTI-VIRAL EFFECT

The observation that trastuzumab was able to elicit a potent anti-viral effect led us to examine pertuzumab, another HER2-targeted antibody with a distinct binding site to trastuzumab on the receptor. Both herceptin and pertuzumab were tested on our cancer cell line panel at a dose of 1000 µg/ml (**Figure 7**). The previously observed anti-viral effect of trastuzumab (Figure 6) was seen in virus sensitive and HER2-high cell lines as was expected and a similar decrease in viral titers was seen with pertuzumab. In addition, the effect of blocking downstream EGFR signaling was examined using the TKI gefitinib, which inhibited viral spread in most of the tested cell lines (**Figure 7**).

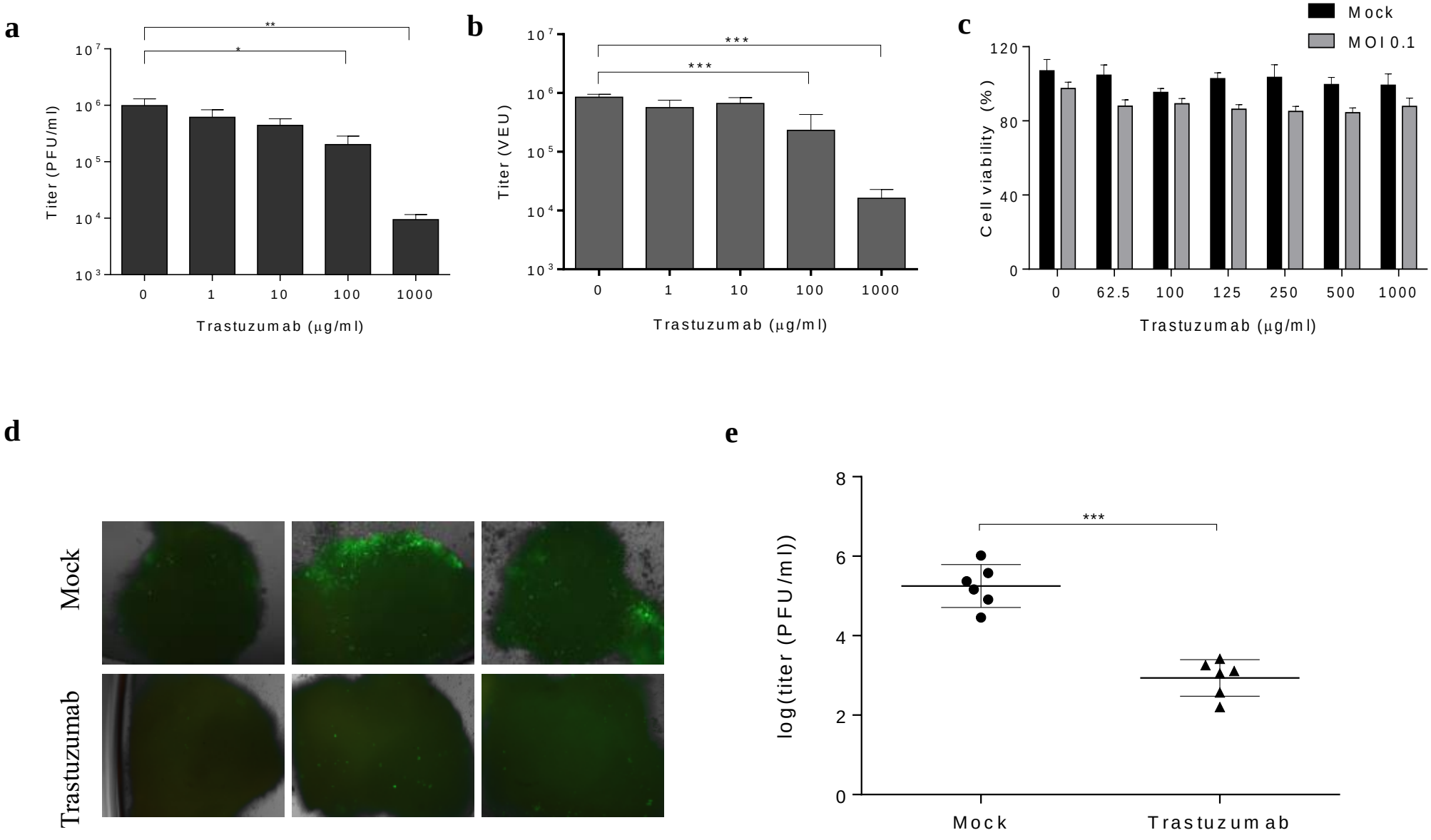
a
Titer (PFU/ml)
Trastuzumab (μg/ml)
b
Titer (VEU)
Trastuzumab (μg/ml)
c
Mock
MOI 0.1
Cell viability (%)
Trastuzumab (μg/ml)
d
Mock
Trastuzumab
e
log(titer (PFU/ml))
Mock
Trastuzumab

Figure 6. Trastuzumab has anti-viral effects on VSVΔ51 titers *in vitro* and *ex vivo*. (a,b) A dose response curve of trastuzumab was performed in 786-0 (a) or SK-OV3 (b) cells; cells were pre-treated with the stated doses of trastuzumab (x-axis) then 4h later infected with VSVΔ51-GFP (a) or –Fluc (b) at an MOI of 0.1. Supernatants were collected 48h post-infection and titered by standard plaque assay (a) or by high-throughput method (b). Data for (a) represent the average value ± SEM from 3 experimental and 3 independent replicates, data for (b) represent the average value ± SD from 3 experimental replicates; * $p< 0.05$, ** $p<0.01$, *** $p<0.001$, one-way ANOVA corrected for multiple comparison with Dunnett's test. **(c)** Alamar Blue was used to assess 786-0 cell viability 48h post-infection with VSVΔ51-Fluc at listed MOIs in combination with increasing doses of trastuzumab (x-axis). Data represent the average value ± SEM from 3 experimental and 3 independent replicates. **(d)** Representative merged GFP, RFP, and bright field images of *ex vivo* SK-OV3 tumour cores pre-treated with trastuzumab 1000µg/ml or mock treated and infected with VSVΔ51-GFP at 5e4 pfu/well. **(e)** Titers from homogenized tumour cores and supernatants 48h post-infection from (d). Data represent 3 experimental replicates from 2 independent experiments; *** $p<0.001$, Student's unpaired T-test.

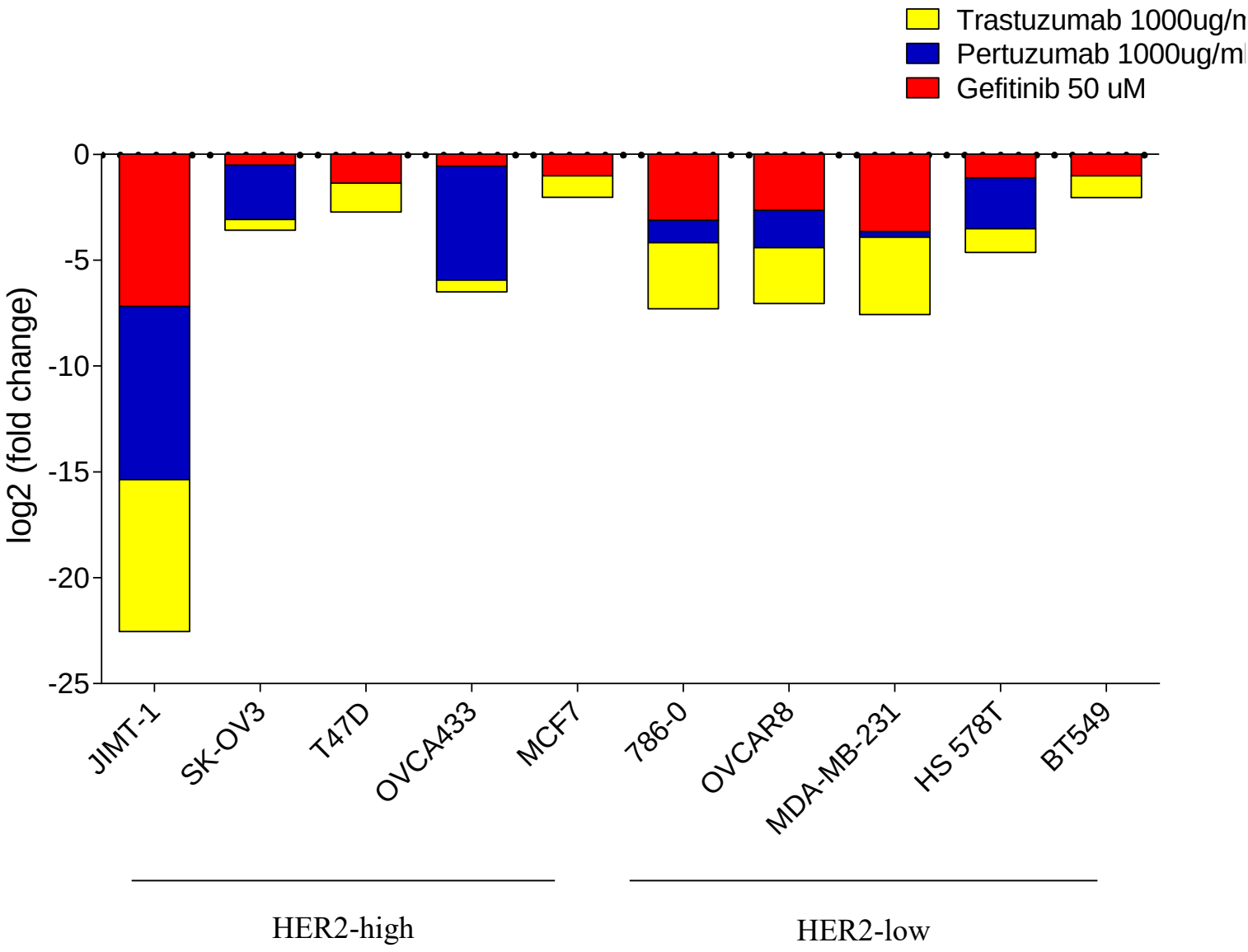
Trastuzumab 1000ug/n
Pertuzumab 1000ug/ml
Gefitinib 50 uM
log2 (fold change)
0
-5
-10
-15
-20
-25
JIMT-1
SK-OV3
T47D
OVCA433
MCF7
786-0
OVCAR8
MDA-MB-231
HS 578T
BT549
HER2-high
HER2-low

Figure 6. Gefitinib and HER2 monoclonal antibodies inhibit virus spreading. Cell lines were pre-treated with 1000 µg/ml of trastuzumab, 1000 µg/ml pertuzumab, or 50 µM gefitinib for 4h at and infected with VSVΔ51-Fluc at MOI 0.1. Supernatants were titered 40h post-infection using a high-throughput method. Data represent the average of 3 experimental replicates ± SD.

3.3- ADCS AS A MEANS TO OVERCOME ANTAGONISM BETWEEN TRASTUZUMAB AND VSVΔ51

3.3.1- CONJUGATION OF TRASTUZUMAB WITH AN MDA OVERCOMES ANTI-VIRAL EFFECTS

We have previously demonstrated that MDAs synergistically increase VSVΔ51 oncolytic activity by decreasing IFNβ secretion and increasing bystander killing (Arulanandam et al., 2015). Based on these observations, we considered that T-DM1 may be a better candidate than trastuzumab for combination therapy with oncolytic VSVΔ51 in OV-resistant cancer cells. To examine this, 786-0 cells were treated with increasing concentrations of T-DM1 and subsequently infected with VSVΔ51 at varying MOIs. A dose dependent increase in VSVΔ51 GFP transgene expression in resistant 786-0 cells was observed at all MOIs (**Figure 8a, top**). Importantly, no dose dependent increase in GFP transgene was observed in normal fibroblasts (**Figure 8a bottom**). This was confirmed by titering the output from 786-0 and GM38 cells following treatment with 1000 µg/ml T-DM1 (**Figure 8b**). Indeed in 786-0 cells, viral titers were significantly increased over untreated control (~200 fold), whereas no such enhancement was seen with GM38 cells. Thus, these data suggest that T-DM1 mediated sensitization to virus infection is cancer specific, consistent with what has been previously observed using MDAs (Arulanandam et al. 2015).

Similar to Figures 5 and 6, a high-throughput titering method was used to further quantify the enhancement of viral titers and cellular cytotoxicity by the combination at various MOIs using a luciferase tagged VSVΔ51. A dose dependent increase in viral titers can be observed with a peak increase of 240-fold over untreated infected cells (**Figure 8c**). Finally, an Alamar Blue assay showed significant enhancement in cellular cytotoxicity was observed starting at doses of 100 µg/ml of T-DM1in the presence of VSVΔ51 relative to drug only treatment (**Figure 8d**).

The combination of T-DM1 with VSVΔ51 was next tested on our panel of cancer cell lines (**Figure 9**). The combination of T-DM1 with VSVΔ51 was able to increase viral titers in some cell lines, most notably in the virus resistant OVCA433 and 786-0 cells. In highly infectable cell lines (e.g. MCF7, see Figure 1a) high baseline titers made it difficult to see increases in viral titers caused by addition of T-DM1.

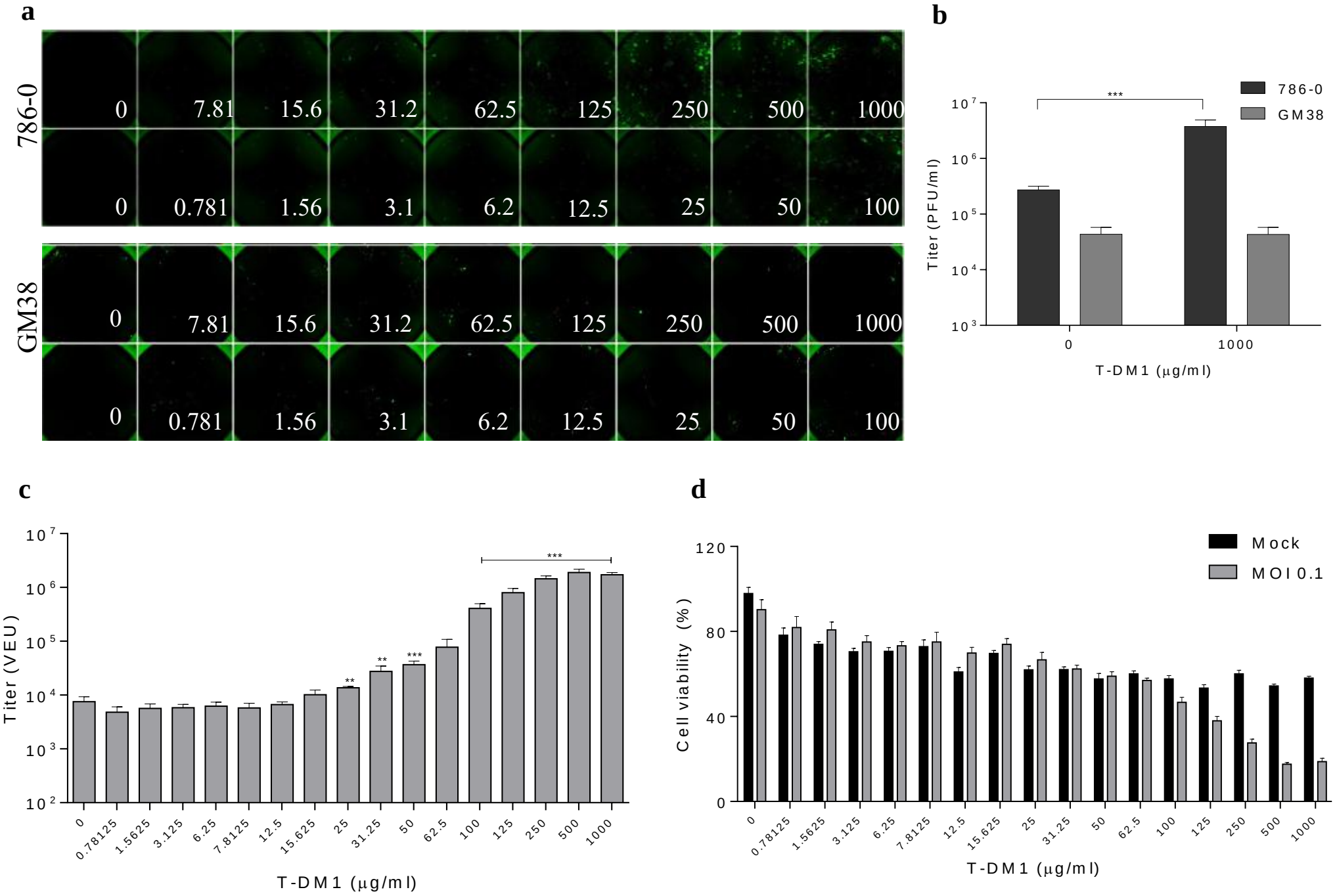
a
786-0
0
7.81
15.6
31.2
62.5
125
250
500
1000
0
0.781
1.56
3.1
6.2
12.5
25
50
100
GM38
0
7.81
15.6
31.2
62.5
125
250
500
1000
0
0.781
1.56
3.1
6.2
12.5
25
50
100
b
786-0
GM38
***
Titer (PFU/ml)
10 7
10 6
10 5
10 4
10 3
0
1000
T-DM1 (μg/ml)
c
Titer (VEU)
10 7
10 6
10 5
10 4
10 3
10 2
***
**
**
***
0
0.78125
1.5625
3.125
6.25
7.8125
12.5
15.625
25
31.25
50
62.5
100
125
250
500
1000
T-DM1 (μg/ml)
d
Mock
MOI 0.1
Cell viability (%)
120
80
40
0
0
0.78125
1.5625
3.125
6.25
7.8125
12.5
15.625
25
31.25
50
62.5
100
125
250
500
1000
T-DM1 (μg/ml)

Figure 8. T-DM1 enhances VSVΔ51 spread in a virus resistant cancer cell line but not in normal fibroblasts. (a) 786-0 human renal carcinoma cells (top) and GM38 primary human fibroblasts (bottom) were pre-treated with increasing doses of T-DM1 as indicated and infected 4h later with VSVΔ51-GFP at an MOI of 0.1. GFP images were taken 24h following infection and representative images are shown for both cell lines. **(b)** Supernatants of 786-0 and cells pre-treated with 0 or 1000 µg/mL of T-DM1 and infected with VSV51-GFP MOI 0.1 were collected and titered by standard plaque assay. Data represent the average value ± SD from 3 experimental replicates, ***$p<0.001$, one-way ANOVA. **(c)** A high-throughput titration method was used to titer supernatants from 786-0 pre-treated with T-DM1 as above and infected with VSVΔ51-Fluc at MOI 0.1. Data represents the average value ± SEM from 3 experimental and 3 independent replicates; **$p<0.1$, ***$p<0.001$, one-way ANOVA corrected for multiple comparison with Dunnett's test. **(d)** Cell viability of panel (c) cells assessed 48h post-infection by Alamar Blue. Data represents the average value ± SEM from 3 experimental and 3 independent replicates.

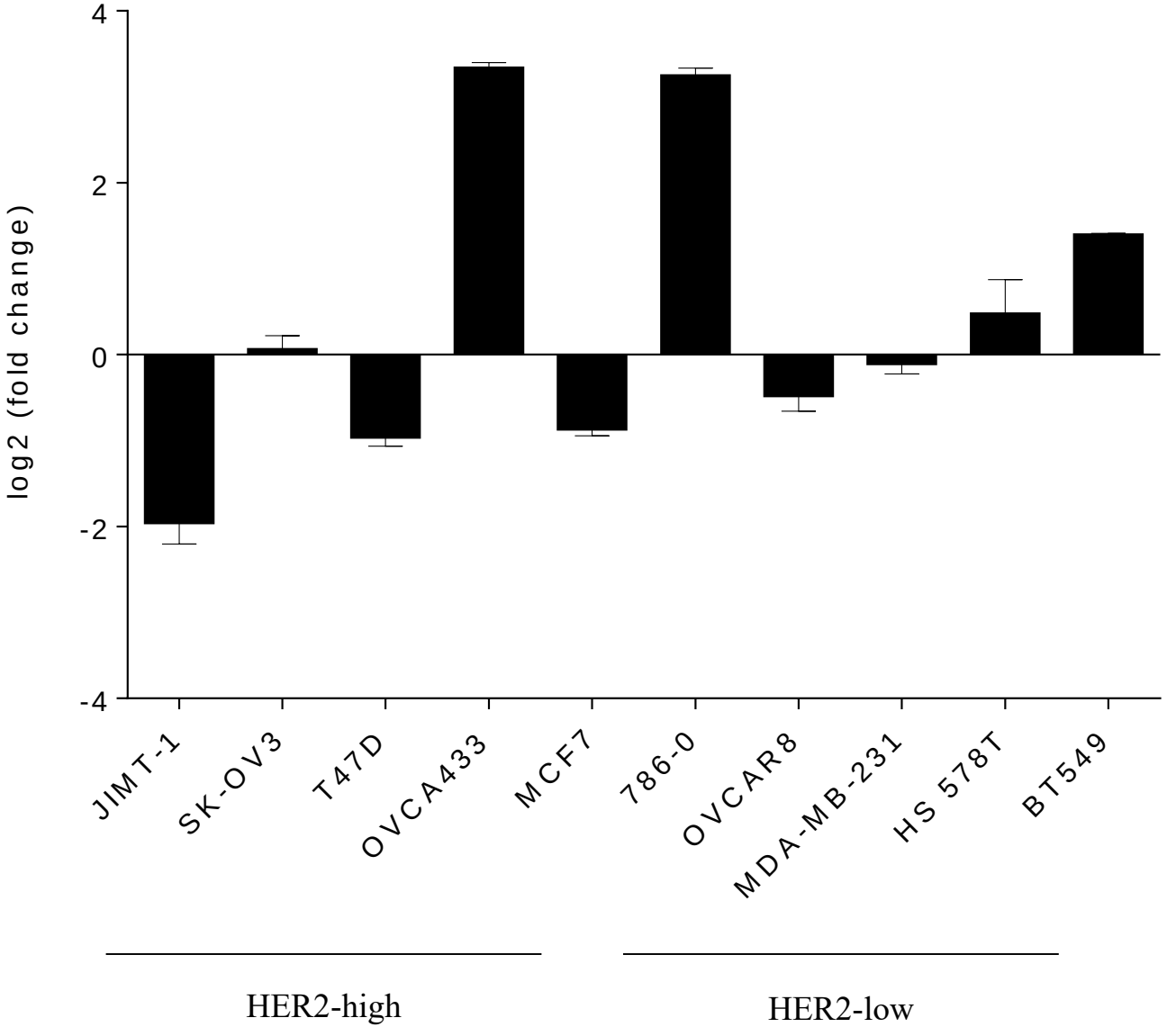
4
2
0
-2
-4
log2 (fold change)
JIMT-1
SK-OV3
T47D
OVCA433
MCF7
786-0
OVCAR8
MDA-MB-231
HS 578T
BT549
HER2-high
HER2-low

Figure 9. T-DM1 enhances VSVΔ51 spread in panel of cancer cell lines. Cell lines were pre-treated for 4h with 1000 µg/ml of T-DM1 and subsequently infected with VSVΔ51-Fluc at MOI 0.1. Samples were titered 40h post-infection by a high-throughput method. Data represent the average of 3 experimental replicates ± SD.

3.3.2- T-DM1 DECREASES IFNβ SECRETION AND INCREASES BYSTANDER POLYNUCLEATION FOLLOWING VSVΔ51 INFECTION

Mechanistically, the enhancement of VSVΔ51-mediated oncolysis by MDAs such as colchicine is associated with MT disruption which leads to both decreased virus-induced IFNβ secretion and increased bystander cell killing (Arulanandam et al., 2015). Similarly, T-DM1treatment of 786-0 cancer cells also led MT destabilization as demonstrated by tubulin staining, an effect that did not occur upon trastuzumab treatment (**Figure 10a**). As expected, a corresponding increase in cell polynucleation, typically associated to mitotic catastrophe events, was also observed in 786-0 cells (0% vs 7%). Normal fibroblasts (GM38) treated with T-DM1 led to MT disruption but did not increase polynucleation likely because of the slower division rate of these cells. As expected, trastuzumab did not alter cell MT structure or polynucleation in GM38 or 786-0 since it is devoid of MDA activity.

The increase in polynucleation caused by T-DM1 was further enhanced by infecting the cells with VSVΔ51 which increased polynucleation frequency from 7 to 33% (**Figure 10b**). The observed enhancement occurred in cells which were not directly infected by the virus, suggesting a bystander killing effect. A modest enhancement in polynucleation was also observed with GM38 cells while trastuzumab treatment had no significant effect on polynucleation following VSV infection.

To assess whether T-DM1 also impacted IFNβ secretion induced by viral infection, 786-0 cells were pre-treated with 100 nM colchicine as a control, 100 µg/ml or 250 µg/ml T-DM1, 100

μg/ml or 1000 μg/ml trastuzumab and subsequently infected with VSVΔ51. Supernatants were collected 20h post-infection and IFNβ secretion was determined by ELISA. Pre-treatment with a dose of 1000 μg/ml of trastuzumab or 250 μg/ml of T-DM1 was able to significantly dampen IFNβ secretion (**Figure 11a**). The selected doses represent those at which the drugs exert their anti-viral (trastuzumab) or pro-viral (T-DM1) effects. Representative GFP images taken at the time of supernatant collection further illustrate the enhancement of virus spreading with T-DM1 (**Figure 11b**). Taken together, these data show that while only T-DM1 has an impact on bystander polynucleation due to the presence of the DM1 moiety, both trastuzumab and T-DM1 can lead to decreased IFNβ secretion, albeit potentially for different reasons as will be discussed below.

a

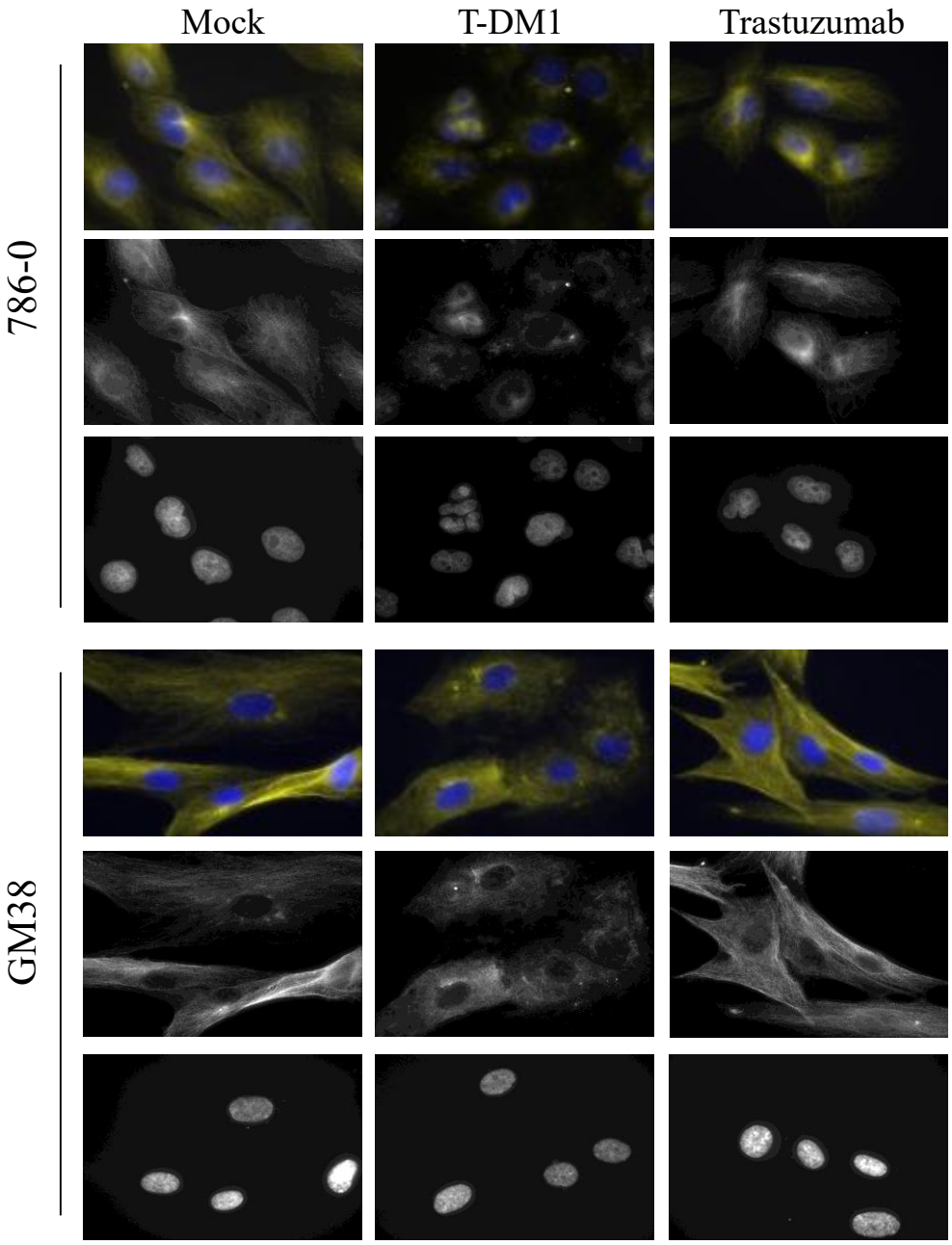
Mock
T-DM1
Trastuzumab
786-0
GM38

b

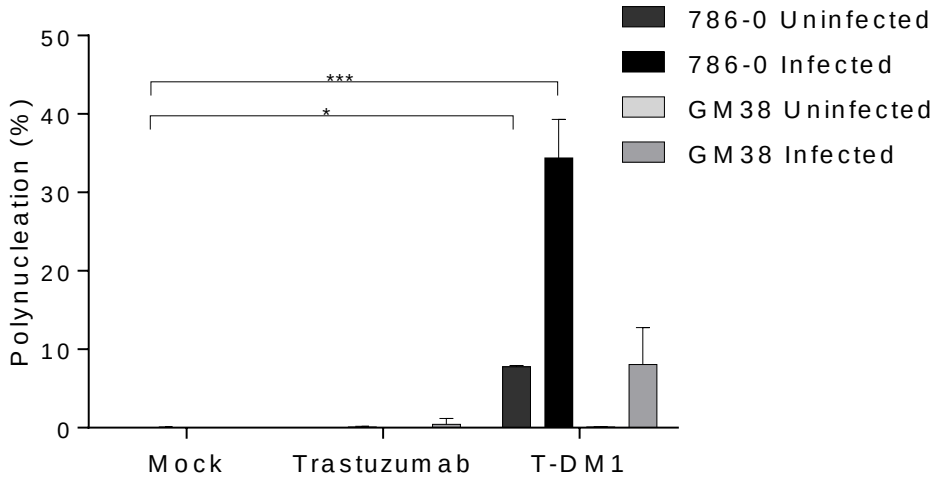
786-0 Uninfected
786-0 Infected
GM38 Uninfected
GM38 Infected
Polynucleation (%)
50
40
30
20
10
0
***
*
Mock
Trastuzumab
T-DM1

Figure 10. T-DM1 increases bystander cell polynucleation following VSVΔ51 infection. **(a)** 786-0 and GM38 cells were treated with 100 nM colchicine, 100 µg/ml T-DM1, 100 µg/ml trastuzumab, or mock treated. Cells were fixed 24h post-infection then subject to immunofluorescent staining, probing for β-tubulin (yellow) and nuclei (DAPI; blue) (n=3). Representative pictures taken at 100X are shown. **(b)** Polynucleation quantification of 786-0 and GM38 cells pre-treated and infected as above. Images were taken 24h post infection and 6 representative frames per experimental condition were counted for polynucleation. Data represent the average value +/- SD from 3 experimental replicates; *$p<0.05$, ***$p<0.001$, one-way ANOVA corrected for multiple comparison with Dunnett's test.

a

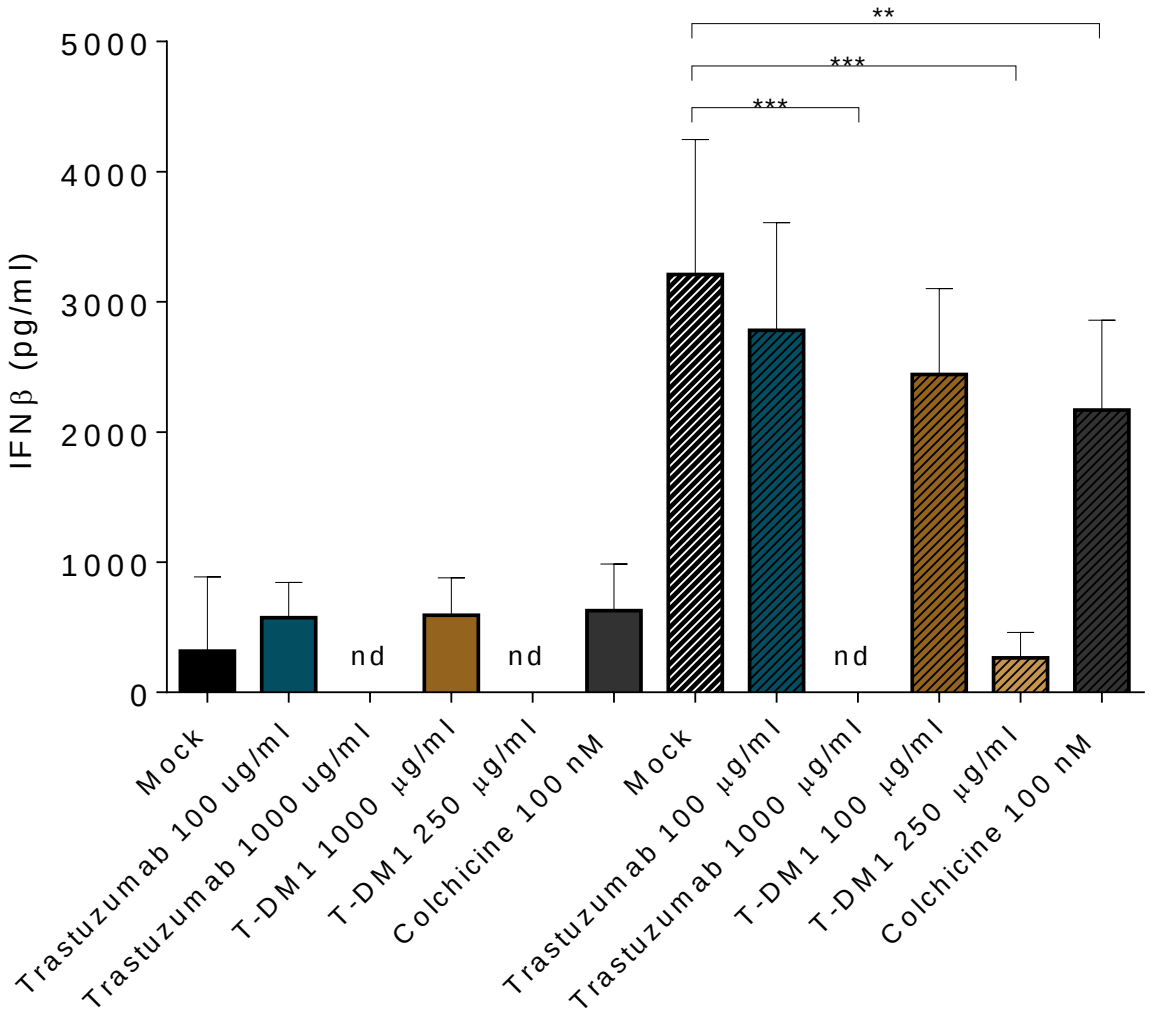
**
***
***
5000
4000
3000
2000
1000
0
IFNβ (pg/ml)
nd
nd
nd
Mock
Trastuzumab 100 ug/ml
Trastuzumab 1000 ug/ml
T-DM1 1000 µg/ml
T-DM1 250 µg/ml
Colchicine 100 nM
Mock
Trastuzumab 100 µg/ml
Trastuzumab 1000 µg/ml
T-DM1 100 µg/ml
T-DM1 250 µg/ml
Colchicine 100 nM

b

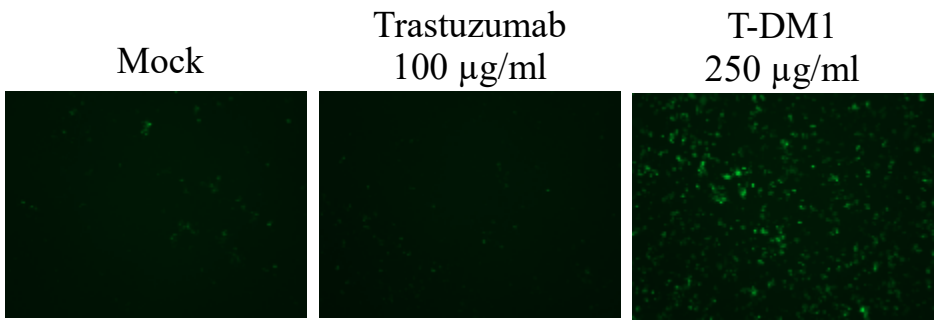
Mock
Trastuzumab
100 µg/ml
T-DM1
250 µg/ml

Figure 11. High dose trastuzumab and T-DM1 decrease IFNβ secretion following infection. (a) 786-0 cells were pre-treated for 4h with 100 or 1000 µg/ml trastuzumab, 100 or 250 µg/ml T-DM1, 100 nM colchicine, or mock treated and were subsequently infected with VSVΔ51-GFP at MOI 0.1 (striped bars), or mock infected (solid bars). Supernatants were collected 20h post-infection and assayed for IFNβ. Data represent the average of at least 3 experimental replicates ± SD; nd= not detectable, **p<0.01, ***p<0.001, one-way ANOVA corrected for multiple comparison with Dunnett's test. **(b)** Representative GFP pictures taken 20h post-infection of above conditions.

4-DISCUSSION

4.1- HER2 ACTIVATION AND SIGNALING POSITIVELY IMPACTS VSVΔ51 INFECTION

Our initial hypothesis was that the mechanism of resistance to anti-HER2 therapies and VSVΔ51 were different and that these modalities could be complementary. Data showed a positive association between HER2 activation and VSVΔ51 infection (**Figure 2**) and suggested that activation of EGFR family receptors would sensitize resistant cell lines to virus. We tested activating ligands of EGFR and found that activation of the EGFR through various ligands was generally able to increase viral spreading (**Figure 5**), suggesting a role for EGFR activation in enhancing virus spread. The finding that abrogation of EGFR signaling by gefitinib, trastuzumab, and pertuzumab was found to be anti-viral further lends support to the importance of EGFR signaling in promoting virus spread (**Figure 7**). Our hypothesis that anti-HER2 therapies could be combined with VSVΔ51 is therefore not supported, as activation of EGFR signaling is clearly important in sensitivity to VSVΔ51.

Interestingly, EGFR activation has been shown to be important for viruses such as adenovirus, hepatitis B and C viruses, vaccinia virus, and human immunodeficiency virus (reviewed in (Zheng et al., 2014)). Although there has been no direct link between EGFR

activation and VSV, over-activation of Ras, a downstream target of EGFR signaling, has been shown to promote VSV oncolysis and is mediated in part by negative regulation of IFNα (Noser et al., 2007). Similarly, work with reovirus in Ras-transformed cells demonstrated that the downstream MEK/ERK pathway was able to inhibit IFNβ expression by blocking retinoic acid-inducible gene 1(RIG-I) signaling (Shmulevitz et al., 2010). Thus, one hypothesis is that blocking of EGFR signaling would relieve the repression on type I IFN production, however this seems unlikely as will be discussed further below.

Interestingly, although all the cell lines tested were responsive to exogenous IFN, there was no association between a cell line's production of IFNβ and VSVΔ51 output (**Figure 3**). The expectation initially was that cell lines which produce low levels of IFNβ in response to virus should be more infectable as they would not be able to elicit a strong anti-viral response. Conversely, cell lines able to secrete substantial IFNβ were predicted to be highly resistant to VSVΔ51 infection. In contrast to the above hypothesis, high IFNβ secreting cells like MCF7 and T47D are highly permissive to VSVΔ51 infection, while the relatively resistant HS 578T cells secrete low levels of IFNβ. These results suggest that a cell's ability to produce IFNβ is not the only determinant for assessing it's response to VSVΔ51.

4.2- POTENTIAL PARTNERS FOR COMBINATION THERAPIES: HER2-TARGETING ANTIBODIES AND VSVΔ51

4.2.1- ANTI-VIRAL EFFECTS OF TRASTUZUMAB

As mentioned above, we had initially hypothesized that the combination between VSVΔ51and trastuzumab could improve treatment efficacy. This was not the case as trastuzumab was found to act as an anti-viral (**Figures 6 and 7**). The mechanism behind this effect has not yet been characterized though several hypotheses can be proposed.

One possibility is that trastuzumab is interfering with virus entry/endocytosis into the cell, which would explain the lack of IFNβ secreted by trastuzumab treated cells in the presence of virus. This possibility would also imply that T-DM1 treatment of cells should also be anti-viral. However this is not supported by our data as T-DM1 enhanced viral spreading and increased viral titers in a number of cell lines (**Figures 8 and 9**).

A second possibility is that trastuzumab interference with downstream EGFR signaling impacts the anti-viral response. As previously mentioned, one of the main effectors of EGFR signaling is Ras. Inhibition of Ras signaling has been previously shown to increase type I IFN secretion (Shmulevitz et al., 2010). We found that IFNβ secretion is in fact decreased by trastuzumab treatment, thus arguing against this possibility (**Figure 11**).

Another possibility is that EGFR family receptor inhibition leads to the activation of an anti-viral factor. This factor should be rapidly induced, since we have shown that a 4h pre-treatment with trastuzumab is able to elicit an anti-viral effect (**Figure 6**). This factor would also have to be overcome or blocked by MDAs, such as DM1. We can likely rule out IFNβ as a mediator of this response given we found that trastuzumab treatment led to decreased IFNβ production 20h following infection with VSVΔ51 (**Figure 11**). While it is a potent anti-viral cytokine, IFNβ kinetics are relatively slow, the secreted protein appearing typically between 8-16h following infection of 786-0 cells (Arulanandam et al., 2015). In this scenario, conditioned media from trastuzumab treated cells, which has been filtered to remove the antibody, should protect naïve cells from VSVΔ51 infection. Filtration using a series of filters of different sizes could be used to aid in the identification of the responsible factor(s).

A more plausible candidate is IL-1β, a pro-inflammatory cytokine that is synthesized as an inactive precursor (pre-IL-1β) and is converted into its active form through caspase-1

cleavage mediated by the activation of the NOD-like receptor family, pyrin domain containing 3 (NLRP3) inflammasome (Chen and Ichinohe, 2015). IL-1β secretion following NLRP3 induction is rapid ~15 minutes, fitting with the timeline of observed protection (**Figure 6**) (Compan et al., 2012). It is possible that inhibition of EGFR signaling triggers (or de-represses) NLRP3 inflammasome activation which would convert pre-IL-1β into the active IL-1β and that this could mediate the observed anti-viral response. Importantly, MDAs such as colchicine and nocodazole have been shown to inhibit the formation of the inflammasome (Misawa et al., 2013). Furthermore, Fcγ antibody receptors (FcγIIIR) signal through to NOD1/NOD2 following binding of IgG to increase pro-IL-1β production (Janczy et al., 2014).

Interestingly, wild-type VSV is able to inhibit pro-IL-1β transcription through the action of its M protein, whereas VSVΔ51, having lost M protein function, induces IL-1β secretion upon replication (Rajan et al., 2011). Given this finding, we would expect that pre-treatment with trastuzumab followed by infection with wild-type VSV would have minimal impact on viral spread since there would be *a priori* absence of pre-IL-1β to be activated.

The possibility that blocking EGFR family receptors, in particular via antibodies, could elicit a rapid anti-viral response may also explain the decrease in IFNβ secretion elicited by trastuzumab treatment, as alluded to above. Indeed, decreased viral growth due to a rapidly acting and IFN-independent anti-viral effect could lead to decreased IFNβ secretion (given there are fewer viruses to activate pattern recognition receptors upstream of IFNβ transcription). We would predict that if the decrease is related to the anti-viral effect, trastuzumab treatment should not increase IFNβ mRNA levels since there is no active viral infection. T-DM1, on the other hand, would be expected to increase IFNβ mRNA levels

since it enhances virus growth. However, similar to what is observed with colchicine (Arulanandam et al., 2015), IFNβ secretion would be decreased due to the presence of the MDA and its negative impact on IFNβ translation (**Figure 11**).

4.2.2- MDA-BASED ADCS AS A MEANS TO OVERCOME TRASTUZUMAB ANTI-VIRAL EFFECTS

Although the combination between VSVΔ51and trastuzumab was shown to be antagonistic, we found that this could be overcome using the MDA based ADC, T-DM1 at least in a subset of cancer cell lines (**Figure 9**). As previously seen with colchicine, the presence of the DM1 moiety was also able to increase bystander killing in the presence of virus (**Figure 10a, b**). Importantly, the presence of the MDA did not alter virus growth in normal fibroblasts (**Figure 8a, b**) nor did it significantly affect bystander killing of those cells (**Figure 10a, b**). This strategy could overcome systemic toxicities associated with MDAs (see introduction) while retaining viral specificity to cancer cells. Our data with T-DM1 is a proof of concept that this strategy is viable, though the anti-viral effect of trastuzumab are likely limiting the impact of DM1. Based on this result, we would expect that conjugation of DM1 or similar MDA to another targeted antibody (e.g. anti-CD30) could lead to an even greater enhancement of VSVΔ51.

4.3- CLINICAL RELEVANCE

The observation that HER2-high cell lines are more susceptible to VSVΔ51 infection (**Figure 2**) may be clinically relevant as it suggests that a tumour's HER2 status could potentially predict future response to VSVΔ51 therapy. Indeed, this is supported by preliminary *in vivo* data showing that HER2-high SK-OV3 tumour bearing mice could be cured of disease with two doses of VSVΔ51 (**Figure 4**), though it would be important to

assess other HER2-high models to better associate the data. It would also be of interest to obtain patient biopsies of tumours with known HER2 status and infect them *ex vivo* with VSVΔ51 to further evaluate HER2 as a potential biomarker.

Antibodies such as trastuzumab, pertuzumab, and T-DM1 can signal through Fcγ receptor leading to ADCC and this effect contributes to the engagement of the host immune system (Gianni, 2008). In metastatic breast cancer patients, a strong natural killer cell activity after neoadjuvant chemotherapy, measured partially through ADCC, was important for the induction of a pathological complete response (Muraro et al., 2015). Thus, ADCC is thought to be an important factor for positive patient outcomes. If it can be confirmed that the observed anti-viral effect of trastuzumab is potentially being mediated by an anti-viral cytokine (e.g. IL-1β), it would be important to establish if this is relevant to ADCC. In this context, we would further speculate that ADCC could be affected by inclusion of the DM1 moiety in T-DM1 given its contrasting positive impact on VSVΔ51 infection.

Our data suggests that at least a subset of patients could benefit from T-DM1 and VSVΔ51 combination therapy (**Figure 9**). Enhancement of VSVΔ51 titers in both HER2-high (OVCA433) and HER2-low (786-0) cell lines is indicative that T-DM1 enhancement may be independent of HER2 status. Thus, both HER2-high and –low tumours could benefit from T-DM1 treatment. Additionally, HER2-low tumours, which would be less permissive to VSVΔ51 infection would further benefit from increased viral spread. Using the combination of T-DM1 with VSVΔ51 could be beneficial in most cases since there may be enhancement in virus spread in resistant tumours, while in permissive tumours robust infection may be accompanied by additional cytotoxicity of the ADC.

4.4- CONCLUSION

Clinical treatment of malignancies is moving in the direction of biotherapeutics and combination therapies. These novel strategies are more targeted than traditional chemotherapeutic agents and also engage the host immune system to produce a lasting anti-tumour response. Using combination therapies to target cancer is a strategy that can help prevent resistance to a single agent and overcome tumour heterogeneity.

Our data show an association between HER2 expression and VSVΔ51 infection and that stimulation of EGFR signaling generally promoted virus growth whereas interference with this signaling, either with TKIs or monoclonal antibodies was detrimental to virus growth. We found that the anti-viral effect mediated by HER2 antibodies could be overcome by ADC treatment and that the MDA moiety was responsible for increased polynucleation and bystander killer effects. Our data also implied that T-DM1 treatment could be effective in both HER2-low and –high cell lines, providing a rationale for VSVΔ51 plus ADC treatment, albeit likely with a different tumour antigen being targeted given the importance of EGFR signaling.

Overall, this work has highlighted the importance of EGFR signaling for oncolytic VSV growth and has outlined a novel strategy combining VSVΔ51 with MDA-loaded ADCs which allow for enhancement of virus spread.

REFERENCES

Agus, D.B., Akita, R.W., Fox, W.D., Lewis, G.D., Higgins, B., Pisacane, P.I., Lofgren, J.A., Tindell, C., Evans, D.P., Maiese, K., Scher, H.I., and Sliwkowski, M.X. (2002). Targeting ligand-activated ErbB2 signaling inhibits breast and prostate tumor growth. Cancer. Cell. *2,* 127-137.

Agus, D.B., Gordon, M.S., Taylor, C., Natale, R.B., Karlan, B., Mendelson, D.S., Press, M.F., Allison, D.E., Sliwkowski, M.X., Lieberman, G., Kelsey, S.M., and Fyfe, G. (2005). Phase I clinical study of pertuzumab, a novel HER dimerization inhibitor, in patients with advanced cancer. J. Clin. Oncol. *23,* 2534-2543.

Alameddine, R.S., Otrock, Z.K., Awada, A., and Shamseddine, A. (2013). Crosstalk between HER2 signaling and angiogenesis in breast cancer: molecular basis, clinical applications and challenges. Curr. Opin. Oncol. *25,* 313-324.

Alemany, R. (2013). Viruses in cancer treatment. Clin. Transl. Oncol. *15,* 182-188.

Arribas, J., Baselga, J., Pedersen, K., and Parra-Palau, J.L. (2011). p95HER2 and breast cancer. Cancer Res. *71,* 1515-1519.

Arulanandam, R., Batenchuk, C., Varette, O., Zakaria, C., Garcia, V., Forbes, N.E., Davis, C., Krishnan, R., Karmacharya, R., Cox, J., *et al.* (2015). Microtubule disruption synergizes with oncolytic virotherapy by inhibiting interferon translation and potentiating bystander killing. Nat. Commun. *6,* 6410.

Barber, G.N. (2005). VSV-tumor selective replication and protein translation. Oncogene *24,* 7710-7719.

Barok, M., Joensuu, H., and Isola, J. (2014). Trastuzumab emtansine: mechanisms of action and drug resistance. Breast Cancer Res. *16,* 209.

Bianchini, G., and Gianni, L. (2014). The immune system and response to HER2-targeted treatment in breast cancer. Lancet Oncol. *15,* e58-68.

BIERMAN, H.R., CRILE, D.M., DOD, K.S., KELLY, K.H., PETRAKIS, N.L., WHITE, L.P., and SHIMKIN, M.B. (1953). Remissions in leukemia of childhood following acute infectious disease: staphylococcus and streptococcus, varicella, and feline panleukopenia. Cancer *6,* 591-605.

Breitbach, C.J., De Silva, N.S., Falls, T.J., Aladl, U., Evgin, L., Paterson, J., Sun, Y.Y., Roy, D.G., Rintoul, J.L., Daneshmand, M., *et al.* (2011). Targeting tumor vasculature with an oncolytic virus. Mol. Ther. *19,* 886-894.

Breitbach, C.J., Paterson, J.M., Lemay, C.G., Falls, T.J., McGuire, A., Parato, K.A., Stojdl, D.F., Daneshmand, M., Speth, K., Kirn, D., *et al.* (2007). Targeted inflammation during oncolytic virus therapy severely compromises tumor blood flow. Mol. Ther. *15,* 1686-1693.

Burotto, M., Chiou, V.L., Lee, J.M., and Kohn, E.C. (2014). The MAPK pathway across different malignancies: a new perspective. Cancer *120,* 3446-3456.

Burstein, H.J., Keshaviah, A., Baron, A.D., Hart, R.D., Lambert-Falls, R., Marcom, P.K., Gelman, R., and Winer, E.P. (2007). Trastuzumab plus vinorelbine or taxane chemotherapy for HER2-overexpressing metastatic breast cancer: the trastuzumab and vinorelbine or taxane study. Cancer *110,* 965-972.

Cantley, L.C. (2002). The phosphoinositide 3-kinase pathway. Science *296,* 1655-1657.

Chen, I.Y., and Ichinohe, T. (2015). Response of host inflammasomes to viral infection. Trends Microbiol. *23,* 55-63.

Chung, C.H., Ely, K., McGavran, L., Varella-Garcia, M., Parker, J., Parker, N., Jarrett, C., Carter, J., Murphy, B.A., Netterville, J., *et al.* (2006). Increased epidermal growth factor receptor gene copy number is associated with poor prognosis in head and neck squamous cell carcinomas. J. Clin. Oncol. *24,* 4170-4176.

Compan, V., Baroja-Mazo, A., Bragg, L., Verkhratsky, A., Perroy, J., and Pelegrin, P. (2012). A genetically encoded IL-1beta bioluminescence resonance energy transfer sensor to monitor inflammasome activity. J. Immunol. *189,* 2131-2137.

Corrigan, P.A., Cicci, T.A., Auten, J.J., and Lowe, D.K. (2014). Ado-trastuzumab emtansine: a HER2-positive targeted antibody-drug conjugate. Ann. Pharmacother. *48,* 1484-1493.

DeVita, V.T.,Jr, and Chu, E. (2008). A history of cancer chemotherapy. Cancer Res. *68,* 8643-8653.

Diallo, J.S., Le Boeuf, F., Lai, F., Cox, J., Vaha-Koskela, M., Abdelbary, H., MacTavish, H., Waite, K., Falls, T., Wang, J., *et al.* (2010). A high-throughput pharmacoviral approach identifies novel oncolytic virus sensitizers. Mol. Ther. *18,* 1123-1129.

Diallo, J.S., Roy, D., Abdelbary, H., De Silva, N., and Bell, J.C. (2011). Ex vivo infection of live tissue with oncolytic viruses. J. Vis. Exp. *(52). pii: 2854. doi,* 10.3791/2854.

Diallo, J.S., Vaha-Koskela, M., Le Boeuf, F., and Bell, J. (2012). Propagation, purification, and in vivo testing of oncolytic vesicular stomatitis virus strains. Methods Mol. Biol. *797,* 127-140.

Dock, G. (1904). The influence of complicating diseases upon leukemia. Am. J. Med. Sci *127,* 563-592.

Dreanic, J., Dhooge, M., Sion, E., Brezault, C., Chaussade, S., and Coriat, R. (2015). Gastric Carcinoma at the Era of Targeted Therapies. Curr. Drug Targets

Dumontet, C., and Jordan, M.A. (2010). Microtubule-binding agents: a dynamic field of cancer therapeutics. Nat. Rev. Drug Discov. *9,* 790-803.

Fillat, C., Maliandi, M.V., Mato-Berciano, A., and Alemany, R. (2014). Combining oncolytic virotherapy and cytotoxic therapies to fight cancer. Curr. Pharm. Des. *20,* 6513-6521.

Finkelshtein, D., Werman, A., Novick, D., Barak, S., and Rubinstein, M. (2013). LDL receptor and its family members serve as the cellular receptors for vesicular stomatitis virus. Proc. Natl. Acad. Sci. U. S. A. *110,* 7306-7311.

Flygare, J.A., Pillow, T.H., and Aristoff, P. (2013). Antibody-drug conjugates for the treatment of cancer. Chem. Biol. Drug Des. *81,* 113-121.

Garcia, V., Krishnan, R., Davis, C., Batenchuk, C., Le Boeuf, F., Abdelbary, H., and Diallo, J.S. (2014). High-throughput titration of luciferase-expressing recombinant viruses. J. Vis. Exp. *(91):51890. doi,* 51890.

Gianni, L. (2008). The "other" signaling of trastuzumab: antibodies are immunocompetent drugs. J. Clin. Oncol. *26,* 1778-1780.

Gutierrez, C., and Schiff, R. (2011). HER2: biology, detection, and clinical implications. Arch. Pathol. Lab. Med. *135,* 55-62.

HAMMON, W.M., YOHN, D.S., CASTO, B.C., and ATCHISON, R.W. (1963). Oncolytic Potentials of Nonhuman Viruses for Human Cancer. I. Effects of Twenty-Four Viruses on Human Cancer Cell Lines. J. Natl. Cancer Inst. *31,* 329-345.

Harrington, K.J., Vile, R.G., Melcher, A., Chester, J., and Pandha, H.S. (2010). Clinical trials with oncolytic reovirus: moving beyond phase I into combinations with standard therapeutics. Cytokine Growth Factor Rev. *21,* 91-98.

Hastie, E., Cataldi, M., Marriott, I., and Grdzelishvili, V.Z. (2013). Understanding and altering cell tropism of vesicular stomatitis virus. Virus Res. *176,* 16-32.

Hudis, C.A. (2007). Trastuzumab--mechanism of action and use in clinical practice. N. Engl. J. Med. *357,* 39-51.

Hurvitz, S.A., Dirix, L., Kocsis, J., Bianchi, G.V., Lu, J., Vinholes, J., Guardino, E., Song, C., Tong, B., Ng, V., Chu, Y.W., and Perez, E.A. (2013). Phase II randomized study of trastuzumab emtansine versus trastuzumab plus docetaxel in patients with human epidermal growth factor receptor 2-positive metastatic breast cancer. J. Clin. Oncol. *31,* 1157-1163.

Ilkow, C.S., Swift, S.L., Bell, J.C., and Diallo, J.S. (2014). From scourge to cure: tumour-selective viral pathogenesis as a new strategy against cancer. PLoS Pathog. *10,* e1003836.

Issell, B.F., and Crooke, S.T. (1978). Maytansine. Cancer Treat. Rev. *5,* 199-207.

Janczy, J.R., Ciraci, C., Haasken, S., Iwakura, Y., Olivier, A.K., Cassel, S.L., and Sutterwala, F.S. (2014). Immune complexes inhibit IL-1 secretion and inflammasome activation. J. Immunol. *193,* 5190-5198.

Jhaveri, K., and Esteva, F.J. (2014). Pertuzumab in the treatment of HER2+ breast cancer. J. Natl. Compr. Canc Netw. *12,* 591-598.

Jiang, H., Gomez-Manzano, C., Rivera-Molina, Y., Lang, F.F., Conrad, C.A., and Fueyo, J. (2015). Oncolytic adenovirus research evolution: from cell-cycle checkpoints to immune checkpoints. Curr. Opin. Virol. *13,* 33-39.

Jordan, M.A. (2002). Mechanism of action of antitumor drugs that interact with microtubules and tubulin. Curr. Med. Chem. Anticancer Agents *2,* 1-17.

Jordan, M.A., and Wilson, L. (2004). Microtubules as a target for anticancer drugs. Nat. Rev. Cancer. *4,* 253-265.

Jordan, M.A., and Wilson, L. (1998). Microtubules and actin filaments: dynamic targets for cancer chemotherapy. Curr. Opin. Cell Biol. *10,* 123-130.

Junttila, T.T., Li, G., Parsons, K., Phillips, G.L., and Sliwkowski, M.X. (2011). Trastuzumab-DM1 (T-DM1) retains all the mechanisms of action of trastuzumab and efficiently inhibits growth of lapatinib insensitive breast cancer. Breast Cancer Res. Treat. *128,* 347-356.

Kampan, N.C., Madondo, M.T., McNally, O.M., Quinn, M., and Plebanski, M. (2015). Paclitaxel and Its Evolving Role in the Management of Ovarian Cancer. Biomed. Res. Int. *2015,* 413076.

Kelly, E., and Russell, S.J. (2007). History of oncolytic viruses: genesis to genetic engineering. Mol. Ther. *15,* 651-659.

Kim, S., Grandis, J.R., Rinaldo, A., Takes, R.P., and Ferlito, A. (2008). Emerging perspectives in epidermal growth factor receptor targeting in head and neck cancer. Head Neck *30,* 667-674.

Krop, I.E., Kim, S.B., Gonzalez-Martin, A., LoRusso, P.M., Ferrero, J.M., Smitt, M., Yu, R., Leung, A.C., Wildiers, H., and TH3RESA study collaborators. (2014). Trastuzumab emtansine versus treatment of physician's choice for pretreated HER2-positive advanced breast cancer (TH3RESA): a randomised, open-label, phase 3 trial. Lancet Oncol. *15,* 689-699.

Lambert, J.M., and Chari, R.V. (2014). Ado-trastuzumab Emtansine (T-DM1): an antibody-drug conjugate (ADC) for HER2-positive breast cancer. J. Med. Chem. *57,* 6949-6964.

Lara, P.N.,Jr, Laptalo, L., Longmate, J., Lau, D.H., Gandour-Edwards, R., Gumerlock, P.H., Doroshow, J.H., Gandara, D.R., and California Cancer Consortium. (2004). Trastuzumab plus docetaxel in HER2/neu-positive non-small-cell lung cancer: a California Cancer Consortium screening and phase II trial. Clin. Lung Cancer. *5,* 231-236.

Lewis Phillips, G.D., Li, G., Dugger, D.L., Crocker, L.M., Parsons, K.L., Mai, E., Blattler, W.A., Lambert, J.M., Chari, R.V., Lutz, R.J., *et al.* (2008). Targeting HER2-positive breast cancer with trastuzumab-DM1, an antibody-cytotoxic drug conjugate. Cancer Res. *68,* 9280-9290.

Lichty, B.D., Breitbach, C.J., Stojdl, D.F., and Bell, J.C. (2014). Going viral with cancer immunotherapy. Nat. Rev. Cancer. *14,* 559-567.

Lichty, B.D., Power, A.T., Stojdl, D.F., and Bell, J.C. (2004). Vesicular stomatitis virus: re-inventing the bullet. Trends Mol. Med. *10,* 210-216.

London, N., and Biggins, S. (2014). Signalling dynamics in the spindle checkpoint response. Nat. Rev. Mol. Cell Biol. *15,* 736-747.

Lopus, M. (2011). Antibody-DM1 conjugates as cancer therapeutics. Cancer Lett. *307,* 113-118.

Lu, Y., Chen, J., Xiao, M., Li, W., and Miller, D.D. (2012). An overview of tubulin inhibitors that interact with the colchicine binding site. Pharm. Res. *29,* 2943-2971.

Mahoney, D.J., and Stojdl, D.F. (2013). Molecular pathways: multimodal cancer-killing mechanisms employed by oncolytic vesiculoviruses. Clin. Cancer Res. *19,* 758-763.

Melcher, A., Parato, K., Rooney, C.M., and Bell, J.C. (2011). Thunder and lightning: immunotherapy and oncolytic viruses collide. Mol. Ther. *19,* 1008-1016.

Miest, T.S., and Cattaneo, R. (2014). New viruses for cancer therapy: meeting clinical needs. Nat. Rev. Microbiol. *12,* 23-34.

Misawa, T., Takahama, M., Kozaki, T., Lee, H., Zou, J., Saitoh, T., and Akira, S. (2013). Microtubule-driven spatial arrangement of mitochondria promotes activation of the NLRP3 inflammasome. Nat. Immunol. *14,* 454-460.

Mukhtar, E., Adhami, V.M., and Mukhtar, H. (2014). Targeting microtubules by natural agents for cancer therapy. Mol. Cancer. Ther. *13,* 275-284.

Muraro, E., Comaro, E., Talamini, R., Turchet, E., Miolo, G., Scalone, S., Militello, L., Lombardi, D., Spazzapan, S., Perin, T., *et al.* (2015). Improved Natural Killer cell activity

and retained anti-tumor CD8(+) T cell responses contribute to the induction of a pathological complete response in HER2-positive breast cancer patients undergoing neoadjuvant chemotherapy. J. Transl. Med. *13,* 204-015-0567-0.

Nahta, R. (2012). Molecular Mechanisms of Trastuzumab-Based Treatment in HER2-Overexpressing Breast Cancer. ISRN Oncol. *2012,* 428062.

Noble, R.L., Beer, C.T., and Cutts, J.H. (1958). Role of chance observations in chemotherapy: *Vinca rosea*. Ann. N. Y. Acad. Sci. *76,* 882-894.

Nogales, E. (2000). Structural insights into microtubule function. Annu. Rev. Biochem. *69,* 277-302.

Noser, J.A., Mael, A.A., Sakuma, R., Ohmine, S., Marcato, P., Lee, P.W., and Ikeda, Y. (2007). The RAS/Raf1/MEK/ERK signaling pathway facilitates VSV-mediated oncolysis: implication for the defective interferon response in cancer cells. Mol. Ther. *15,* 1531-1536.

Oroudjev, E., Lopus, M., Wilson, L., Audette, C., Provenzano, C., Erickson, H., Kovtun, Y., Chari, R., and Jordan, M.A. (2010). Maytansinoid-antibody conjugates induce mitotic arrest by suppressing microtubule dynamic instability. Mol. Cancer. Ther. *9,* 2700-2713.

Padhy, L.C., Shih, C., Cowing, D., Finkelstein, R., and Weinberg, R.A. (1982). Identification of a phosphoprotein specifically induced by the transforming DNA of rat neuroblastomas. Cell *28,* 865-871.

Paplomata, E., and O'Regan, R. (2014). The PI3K/AKT/mTOR pathway in breast cancer: targets, trials and biomarkers. Ther. Adv. Med. Oncol. *6,* 154-166.

Parato, K.A., Senger, D., Forsyth, P.A., and Bell, J.C. (2005). Recent progress in the battle between oncolytic viruses and tumours. Nat. Rev. Cancer. *5,* 965-976.

Parker, A.L., Kavallaris, M., and McCarroll, J.A. (2014). Microtubules and their role in cellular stress in cancer. Front. Oncol. *4,* 153.

Pasquinucci, G. (1971). Possible effect of measles on leukaemia. Lancet *1,* 136.

Peddi, P.F., and Hurvitz, S.A. (2014). Ado-trastuzumab emtansine (T-DM1) in human epidermal growth factor receptor 2 (HER2)-positive metastatic breast cancer: latest evidence and clinical potential. Ther. Adv. Med. Oncol. *6,* 202-209.

Pelletier P.J., C.J.B. (1820). Examen chimique des plusieurs végétaux de la famille des colchicées, et du principe actif qu'ils renferment. [Cévadille (veratrum sabadilla); hellébore blanc (veratrum album); colchique commun (colchicum autumnale)]. Annales De Chimie Et De Physique *14,* 69-81.

Perez, E.A., Hurvitz, S.A., Amler, L.C., Mundt, K.E., Ng, V., Guardino, E., and Gianni, L. (2014). Relationship between HER2 expression and efficacy with first-line trastuzumab emtansine compared with trastuzumab plus docetaxel in TDM4450g: a randomized phase II study of patients with previously untreated HER2-positive metastatic breast cancer. Breast Cancer Res. *16*, R50.

Pol, J., Bloy, N., Obrist, F., Eggermont, A., Galon, J., Cremer, I., Erbs, P., Limacher, J.M., Preville, X., Zitvogel, L., Kroemer, G., and Galluzzi, L. (2014). Trial Watch:: Oncolytic viruses for cancer therapy. Oncoimmunology *3*, e28694.

Press, M.F., and Lenz, H.J. (2007). EGFR, HER2 and VEGF pathways: validated targets for cancer treatment. Drugs *67*, 2045-2075.

Quiroz, E., Moreno, N., Peralta, P.H., and Tesh, R.B. (1988). A human case of encephalitis associated with vesicular stomatitis virus (Indiana serotype) infection. Am. J. Trop. Med. Hyg. *39*, 312-314.

Rajan, J.V., Rodriguez, D., Miao, E.A., and Aderem, A. (2011). The NLRP3 inflammasome detects encephalomyocarditis virus and vesicular stomatitis virus infection. J. Virol. *85*, 4167-4172.

Reddy, K.B., Nabha, S.M., and Atanaskova, N. (2003). Role of MAP kinase in tumor progression and invasion. Cancer Metastasis Rev. *22*, 395-403.

Regan, A.D., and Whittaker, G.R. (2013). Entry of rhabdoviruses into animal cells. Adv. Exp. Med. Biol. *790*, 167-177.

Reif, J.S., Webb, P.A., Monath, T.P., Emerson, J.K., Poland, J.D., Kemp, G.E., and Cholas, G. (1987). Epizootic vesicular stomatitis in Colorado, 1982: infection in occupational risk groups. Am. J. Trop. Med. Hyg. *36*, 177-182.

Risinger, A.L., Giles, F.J., and Mooberry, S.L. (2009a). Microtubule dynamics as a target in oncology. Cancer Treat. Rev. *35*, 255-261.

Risinger, A.L., Giles, F.J., and Mooberry, S.L. (2009b). Microtubule dynamics as a target in oncology. Cancer Treat. Rev. *35*, 255-261.

Russell, S.J. (2002). RNA viruses as virotherapy agents. Cancer Gene Ther. *9*, 961-966.

Scheuer, W., Friess, T., Burtscher, H., Bossenmaier, B., Endl, J., and Hasmann, M. (2009). Strongly enhanced antitumor activity of trastuzumab and pertuzumab combination treatment on HER2-positive human xenograft tumor models. Cancer Res. *69*, 9330-9336.

Schmidt, M. (2014). Chemotherapy in early breast cancer: when, how and which one? Breast Care. (Basel) *9*, 154-160.

Shmulevitz, M., Pan, L.Z., Garant, K., Pan, D., and Lee, P.W. (2010). Oncogenic Ras promotes reovirus spread by suppressing IFN-beta production through negative regulation of RIG-I signaling. Cancer Res. *70,* 4912-4921.

Slamon, D.J., Leyland-Jones, B., Shak, S., Fuchs, H., Paton, V., Bajamonde, A., Fleming, T., Eiermann, W., Wolter, J., Pegram, M., Baselga, J., and Norton, L. (2001). Use of chemotherapy plus a monoclonal antibody against HER2 for metastatic breast cancer that overexpresses HER2. N. Engl. J. Med. *344,* 783-792.

Sliwkowski, M.X. (2003). Ready to partner. Nat. Struct. Biol. *10,* 158-159.

Slobodnick, A., Shah, B., Pillinger, M.H., and Krasnokutsky, S. (2015). Colchicine: old and new. Am. J. Med. *128,* 461-470.

SOUTHAM, C.M., and MOORE, A.E. (1952). Clinical studies of viruses as antineoplastic agents with particular reference to Egypt 101 virus. Cancer *5,* 1025-1034.

SOUTHAM, C.M., and MOORE, A.E. (1951). West Nile, Ilheus, and Bunyamwera virus infections in man. Am. J. Trop. Med. Hyg. *31,* 724-741.

Stojdl, D.F., Lichty, B.D., tenOever, B.R., Paterson, J.M., Power, A.T., Knowles, S., Marius, R., Reynard, J., Poliquin, L., Atkins, H., *et al.* (2003). VSV strains with defects in their ability to shutdown innate immunity are potent systemic anti-cancer agents. Cancer. Cell. *4,* 263-275.

Swain, S.M., Baselga, J., Kim, S.B., Ro, J., Semiglazov, V., Campone, M., Ciruelos, E., Ferrero, J.M., Schneeweiss, A., Heeson, S., *et al.* (2015). Pertuzumab, trastuzumab, and docetaxel in HER2-positive metastatic breast cancer. N. Engl. J. Med. *372,* 724-734.

Tafe, L.J., and Tsongalis, G.J. (2011). The human epidermal growth factor receptor 2 (HER2). Clin. Chem. Lab. Med. *50,* 23-30.

Taqi, A.M., Abdurrahman, M.B., Yakubu, A.M., and Fleming, A.F. (1981). Regression of Hodgkin's disease after measles. Lancet *1,* 1112.

Tesh, R.B., Peralta, P.H., and Johnson, K.M. (1969). Ecologic studies of vesicular stomatitis virus. I. Prevalence of infection among animals and humans living in an area of endemic VSV activity. Am. J. Epidemiol. *90,* 255-261.

Valachis, A., Mauri, D., Polyzos, N.P., Chlouverakis, G., Mavroudis, D., and Georgoulias, V. (2011). Trastuzumab combined to neoadjuvant chemotherapy in patients with HER2-positive breast cancer: a systematic review and meta-analysis. Breast *20,* 485-490.

Verma, S., Miles, D., Gianni, L., Krop, I.E., Welslau, M., Baselga, J., Pegram, M., Oh, D.Y., Dieras, V., Guardino, E., *et al.* (2012). Trastuzumab emtansine for HER2-positive advanced breast cancer. N. Engl. J. Med. *367,* 1783-1791.

Webb, P.A., Monath, T.P., Reif, J.S., Smith, G.C., Kemp, G.E., Lazuick, J.S., and Walton, T.E. (1987). Epizootic vesicular stomatitis in Colorado, 1982: epidemiologic studies along the northern Colorado front range. Am. J. Trop. Med. Hyg. *36,* 183-188.

Welslau, M., Dieras, V., Sohn, J.H., Hurvitz, S.A., Lalla, D., Fang, L., Althaus, B., Guardino, E., and Miles, D. (2014). Patient-reported outcomes from EMILIA, a randomized phase 3 study of trastuzumab emtansine (T-DM1) versus capecitabine and lapatinib in human epidermal growth factor receptor 2-positive locally advanced or metastatic breast cancer. Cancer *120,* 642-651.

Yohn, D.S., Hammon, W.M., Atchison, R.W., and Casto, B.C. (1968). Oncolytic potentials of nonhuman viruses for human cancer. II. Effects of five viruses on heterotransplantable human tumors. J. Natl. Cancer Inst. *41,* 523-529.

Zaczek, A., Brandt, B., and Bielawski, K.P. (2005). The diverse signaling network of EGFR, HER2, HER3 and HER4 tyrosine kinase receptors and the consequences for therapeutic approaches. Histol. Histopathol. *20,* 1005-1015.

Zhao, L., and Vogt, P.K. (2008). Class I PI3K in oncogenic cellular transformation. Oncogene *27,* 5486-5496.

Zheng, K., Kitazato, K., and Wang, Y. (2014). Viruses exploit the function of epidermal growth factor receptor. Rev. Med. Virol. *24,* 274-286.

CONTRIBUTION FROM COLLABORATORS

Oliver assisted with the Kadcyla dose response, screening of cell lines for VSVΔ51 infectivity and the EGFRHER2 and TKI screen as well as the supernatant transfer experiments.

Rozanne assisted with EGFR/HER2 drug screen

Colin Davis performed data analysis of all high-throughput experiments

Andrew Chen and Theresa Falls were invaluable for all *in vivo* experiments.

APPENDICES

APPENDIX 1

High-throughput Titration of Luciferase-expressing Recombinant Viruses

Vanessa Garcia, Ramya Krishnan, Colin Davis, Cory Batenchuk, Fabrice Le Boeuf, Hesham Abdelbary, Jean-Simon Diallo

Author Contribution: Helped in the conception, development, and protocol optimization of the high-throughput titration method. Contributed significantly to manuscript writing, editing, and preparation.

Journal of Visualized Experiments

www.jove.com

Video Article

High-throughput Titration of Luciferase-expressing Recombinant Viruses

Vanessa Garcia[1,2], Ramya Krishnan[1,2], Colin Davis[1,2], Cory Batenchuk[1,2], Fabrice Le Boeuf[1,3], Hesham Abdelbary[1,3], Jean-Simon Diallo[1,2] [1]Center for Innovative Cancer Research, Ottawa Hospital Research Institute [2]Department of Biochemistry, Microbiology and Immunology, Faculty of Medicine, University of Ottawa [3]Faculty of Medicine, University of Ottawa

Correspondence to: Jean-Simon Diallo at jsdiallo@ohri.ca

URL:
http://www.jove.com/video/51890
DOI:
doi:10.3791/51890

Keywords: Virology, Issue 91, titration, virus, plaque assay, high-throughput, transgene, luciferase, automated, cytotoxicity assay, Vesicular Stomatitis Virus, Herpes Simplex virus, Vaccinia virus, Adeno-Associated virus

Date Published: 9/19/2014

Citation: Garcia, V., Krishnan, R., Davis, C., Batenchuk, C., Le Boeuf, F., Abdelbary, H., Diallo, J.S. High-throughput Titration of Luciferase-expressing Recombinant Viruses. *J. Vis. Exp.* (91), e51890, doi:10.3791/51890 (2014).

Abstract

Standard plaque assays to determine infectious viral titers can be time consuming, are not amenable to a high volume of samples, and cannot be done with viruses that do not form plaques. As an alternative to plaque assays, we have developed a high-throughput titration method that allows for the simultaneous titration of a high volume of samples in a single day. This approach involves infection of the samples with a Firefly luciferase tagged virus, transfer of the infected samples onto an appropriate permissive cell line, subsequent addition of luciferin, reading of plates in order to obtain luminescence readings, and finally the conversion from luminescence to viral titers. The assessment of cytotoxicity using a metabolic viability dye can be easily incorporated in the workflow in parallel and provide valuable information in the context of a drug screen. This technique provides a reliable, high-throughput method to determine viral titers as an alternative to a standard plaque assay.

Video Link

The video component of this article can be found at http://www.jove.com/video/51890/

Introduction

Classical viral plaque assays continue to be a mainstay in virus research even though they can be notoriously time-consuming and constitute a significant bottleneck to obtaining results from experiments. More rapid indirect virus quantification methods have emerged including quantitative polymerase chain reaction (qPCR), ELISA, and flow cytometry[1-4]. Recent innovations such as the Virocyt virus counter can directly count viruses using advanced flow sorting technology and through a combination of protein and DNA/RNA dyes[5]. While all of these methods have undoubtedly quickened the pace of virus research, each method has its advantages and drawbacks. For example, qPCR can allow for quantification of specific viral genome sequence but cannot effectively discriminate infectious from defective virions[6]. ELISAs can be very specific however require a suitable antibody against the desired target viral protein and can be very expensive. While flow cytometry technology offers many advantages and has improved significantly, throughput and accessibility to highly specialized equipment nonetheless remains a hurdle. Importantly, all of these techniques are not ideally suited for high-throughput screening, for which the ease and time requirement of the virus quantification step is of critical importance.

Here we describe a high-throughput and easily automatable technique to titer viruses that express a Firefly luciferase (Fluc) transgene. This method generates approximate viral titers in a test sample based on luminescence signal reads through the parallel use of a standard curve of known amounts of virus. Samples containing unknown quantities of luciferase-expressing virus are transferred on to a permissive “plaquing” cell line in parallel with the standard virus dilution

curve and virus-associated luminescence is read after a few hours incubation time. This allows for rapid, quantitative, often same-day generation of results, unlike classic plaque assay protocols which typically require several days of incubation in order to manually count visible plaques[7-9].

The protocol outlines the steps of our titration method using oncolytic Vesicular Stomatitis Virus encoding a Fluc transgene (VSVΔ51-Fluc) as an example and provides an overview of 1. Sample preparation 2. The plating of a permissive cell line for virus titration using an automated dispenser 3. The preparation of the viral standard curve 4. The transfer of the sample supernatants onto the permissive cell line using a 96-well manual pipettor 5. The assessment of sample cytotoxicity using a cell viability reagent 6. The preparation of the luciferin substrate 7. Reading of bioluminescence and 8. Data analysis.

Protocol

1. Sample Preparation

1. Obtain samples containing luciferase-expressing virus (herein VSVΔ51-Fluc as an example) for titration and transfer into 96-well plates. Alternately, perform infections in 96-well tissue culture plates and use supernatants directly.
2. Leave two columns untreated for the inclusion of standard curves. For experiments done directly in 96-well plates, titer at the end of the experiment (40 hr post-infection) or store at -80 °C and titer at a later date.

2. Preparation of Permissive Cells for Virus Titration

1. 24 hr prior to titering, prepare a suspension of Vero cells at a concentration of 2.5 x 10^5 cells/ml in Dulbecco's modified eagle medium (DMEM) containing 10% fetal bovine serum (FBS), 30 mM HEPES, and 1% penicillin/streptomycin. NOTE: Although this protocol uses Vero cells, any suitable permissive cell line for VSV infection could be used.
2. Seed 2.5 x 10^4 cells (100 µl) in 96-well white solid flat-bottom plates using a microplate dispenser.
    1. Prepare 12 ml of cell suspension per plate plus 5 ml for priming.
    2. Clean microplate dispenser cassette by flushing the tubing with 50 ml of sterile water.
    3. Fill the microplate dispenser lines with cell suspension and let 5 ml of cell suspension flow through.
    4. Select a program that will dispense 100 µl in each well of a white-walled 96-well plate. Dispense, and repeat as necessary for additional plates. Also seed a few wells in a 96-well clear flat-bottom plate if opaque-bottom white-walled plates are used for verification of cell health and density.
    5. When finished, flush cells back into original container. Clean the cassette by running 50 ml of 70% ethanol followed by 50 ml of warm sterile water through the tubing.
    6. Make sure cassette and tubing are appropriately cleaned between uses.
3. Incubate cells for 24 hr at 37 °C in a humidified 5% CO_2 incubator.

3. Preparation of Viral Standard Curve

1. Prepare a standard curve of VSVΔ51-Fluc in serum-free DMEM such that the final concentration of plaque forming units (pfu) per ml after transfer onto Vero cells is as follows: 10^8 pfu/ml, 10^7 pfu/ml, 10^6 pfu/ml, 10^5 pfu/ml, 10^4 pfu/ml, 10^3 pfu/ml, 10^2 pfu/ml, and 10^1 pfu/ml. Prepare 50 µl of each concentration per plate of Vero cells plus an extra 10%.
   NOTE: Titer of the luciferase virus stock will need to be assessed in a classical way[10] in order to generate a standard curve that will allow for absolute quantification. Otherwise relative quantification can be achieved without precise titer information by arbitrarily setting viral titer based on dilution steps. For example the first dilution of the standard curve may be set to 10^8 viral units and the following 1/10 dilution to 10^7 and so on. In this context, one should express values as a fold-change compared to a pre-determined sample as absolute quantification will not be accurate.

4. Transfer of Sample Supernatants onto Permissive Cells

1. Check Vero cells plated in the clear-bottom 96-well plate under a light microscope to confirm that monolayers are at least 95% confluent.
2. Transfer 25 µl of sample supernatant onto Vero cells seeded in white-walled plates. Do not transfer supernatants into the 2 columns designated for standard curves. NOTE: This can be done simultaneously for all wells on a single plate using a 96-channel liquid handler.
3. Using an 8- or 12-channel multi-channel pipettor, add 25 µl of each dilution of the standard curve prepared in Step 3 to the Vero cells in the 2 designated columns.
4. Centrifuge plates for 5 min at 430 x g at RT.
5. Incubate for 5 hr at 37 °C in a humidified 5% CO_2 incubator.

5. Assessment of Cell Viability

1. NOTE: When starting from supernatants obtained from infection experiments done in clear 96-well plates, sample viability can be assessed prior to quantification with a cell viability indicator dye such as resazurin.
2. Add resazurin in an amount equal to 10% of the volume in each well of the 96-well plate of samples containing virus and cells. Include cell-only controls as well as media-only control to determine values for 100% and 0% viability respectively.
3. After 2-4 hr (incubation time will vary depending on cell type and on the concentration of commercially available or reconstituted powder of the dye), read and record the signal using a fluorescence plate reader (530-560 excitation, 590 emission). Report cell viability for a sample according to the formula Relative Metabolic Activity = ((Test sample signal - negative control signal) / (Cell only control signal - negative control signal)) x 100%

6. Preparation of the Luciferin Substrate

1. 30 min before the end of the 5 hr incubation, prepare the luciferin to obtain a 2 mg/ml solution in sterile phosphate buffered saline (PBS). Prepare 2.5 ml per plate plus an extra 2 ml. Protect solution from light. NOTE: The luciferin may also be prepared earlier in the day and stored at 4 °C until use.

7. Reading Bioluminescence

1. After the 5 hr incubation period, add 25 µl of luciferin to each well of Vero cells in the white solid plates. Add luciferin manually or with an automated dispenser integrated in the luminometer. NOTE: The use of an instrument with only single and end point reads may require the addition of a luciferase compatible lysis buffer prior to adding the luciferin substrate to improve consistency.
2. Read the plates with the following parameters:
    1. Shake for 5 sec.
    2. Wait 30 sec.
    3. Read luminescence at an appropriate fixed sensitivity / exposure value. If the option is available on the instrument, use multi-point reads (*e.g.,* 3 x 3 matrix) to improve accuracy.
3. Record and save the quantified bioluminescent intensity.
4. If an automated dispenser was used to add luciferin purge the luciferin and prime the lines with warm sterile water.

8. Data Analysis

1. For accurate results, solve the non-linear regression to generate a Hill equation from the standard curves. Apply this equation to the titered samples to calculate viral expression units. Some viruses or situations may produce a standard curve with a linear relationship; in this case solve for a linear equation.

Representative Results

A summary of the workflow describing the high-throughput method is illustrated in **Figure 1**. **Figure 2** shows the results of a typical standard curve ofVSVΔ51-Fluc. Four-parameter non-linear regression analysis generated a Hill plot from which unknown input pfu (estimate of viral titer) can be interpolated. These estimated titers are termed viral expression units (VEU). **Figure 3A** shows VEUs and titers obtained by performing a standard plaque assay with the same samples[10]. Samples originated from an experiment where various chemicals were used to enhance the replication and spread of VSVΔ51-Fluc in 786-0 cells. VEUs interpolated from the standard curve must be multiplied by a factor which is based on the dilution of sample supernatants being transferred on to Vero cells (in this case, the dilution factor is 5). The linear correlation between titers and VEU is shown in **Figure 3B** with an R^2 of 0.8083 and a Pearson's r score of 0.899 ($p < 0.0001$). In **Figure 4**, typical cell cytotoxicity data obtained from a metabolic assay is shown for 786-0 cells treated with chemicals prior to infection with VSVΔ51-Fluc. Finally, **Figure 5** shows typical standard curves obtained with various viruses (Herpes Simplex Virus (HSV), Vaccinia virus, and Adeno-Associated Virus (AAV), all expressing Firefly luciferase) and describes incubation times and freeze-thaw cycles, as required.

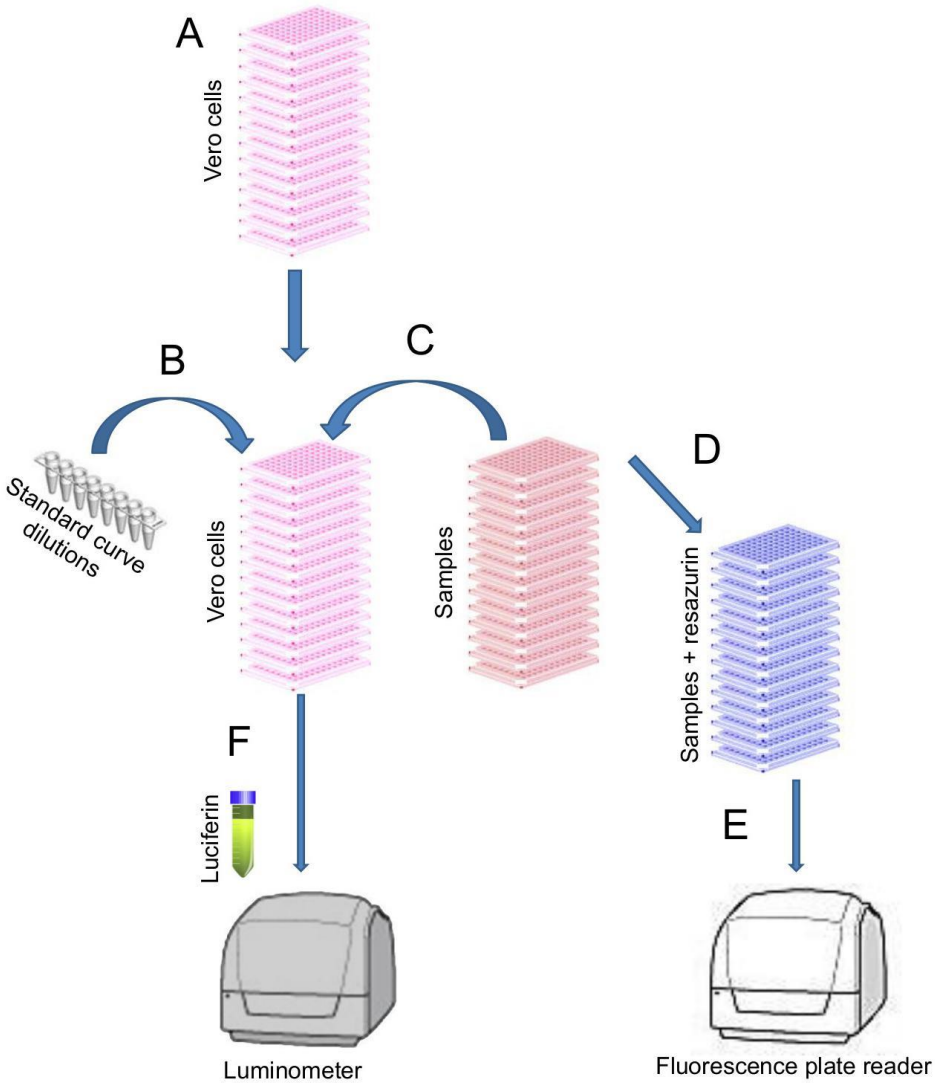

Figure 1. Workflow of high-throughput virus titering and cytotoxicity assay using VSVΔ51-Fluc. (A) Seed 2.5 x 10^4 Vero cells per well (100 µl) and incubate at 37 °C. **(B)** 24 hr later transfer 25 µl of standard curve on to Vero cells (2 columns per plate). **(C)** Transfer 25 µl of samples to be titered on to remaining Vero cells. Centrifuge plates and incubate at 37 °C. **(D)** In an amount equal to 10% of the volume in the well, add resazurin reagent to the plate containing the original samples. Incubate plates at 37 °C. **(E)** After 3 hr, read and record fluorescence and assess cytotoxicity. **(F)** After 5 hr, add 25 µl of 2 mg/ml solution of luciferin to each well of Vero cells. Read luminescence and calculate Viral Expression Units.

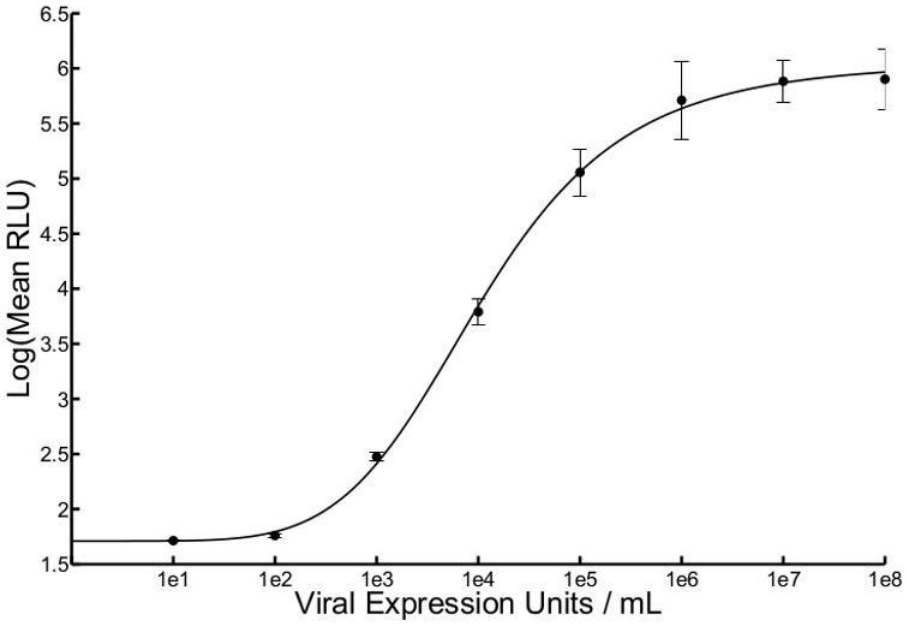

Figure 2. Expected standard curve of VSVΔ51-Fluc. Luciferase expression was measured 5 hr post supernatant transfer at five different points within a well using a luminometer and bioluminescence was expressed in mean relative light units (RLU). Mean RLU was plotted against known input pfu/ml to solve the non-linear regression and generate a Hill equation. The average of two replicate curves and standard error bars are shown (r^2= 0.9993).

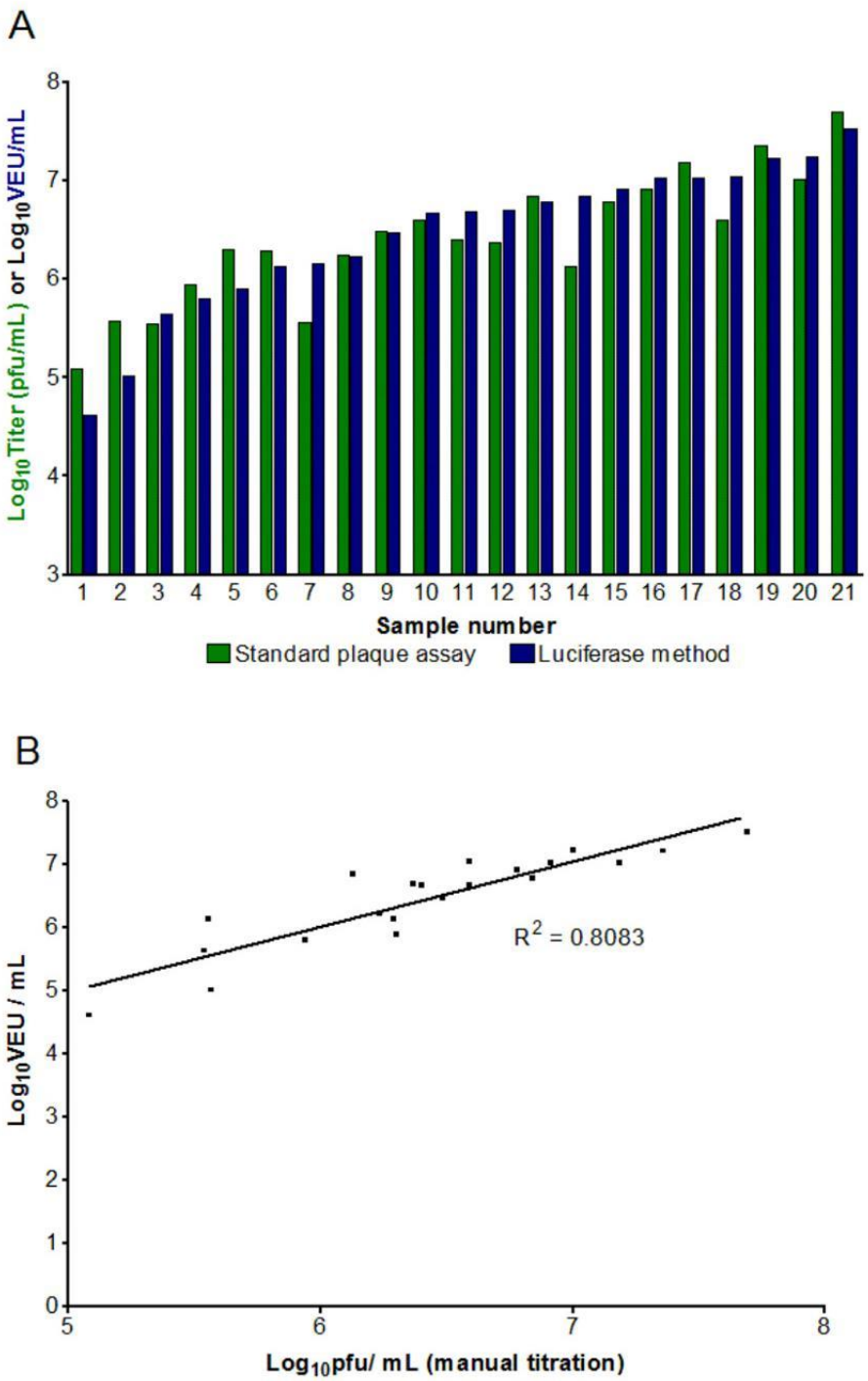

Figure 3. Comparison of standard plaque assay titers with those obtained by high-throughput method. (A) Viral titers in pfu/ml obtained by standard plaque assay on Vero cells were compared with calculated viral titers (VEU/ml) from the same samples titered using the high-throughput luciferase assay. **(B)** Linear relationship between VEU/ml and titer obtained via standard plaque assay. Linear regression curve and coefficient of determination (R^2) are shown.

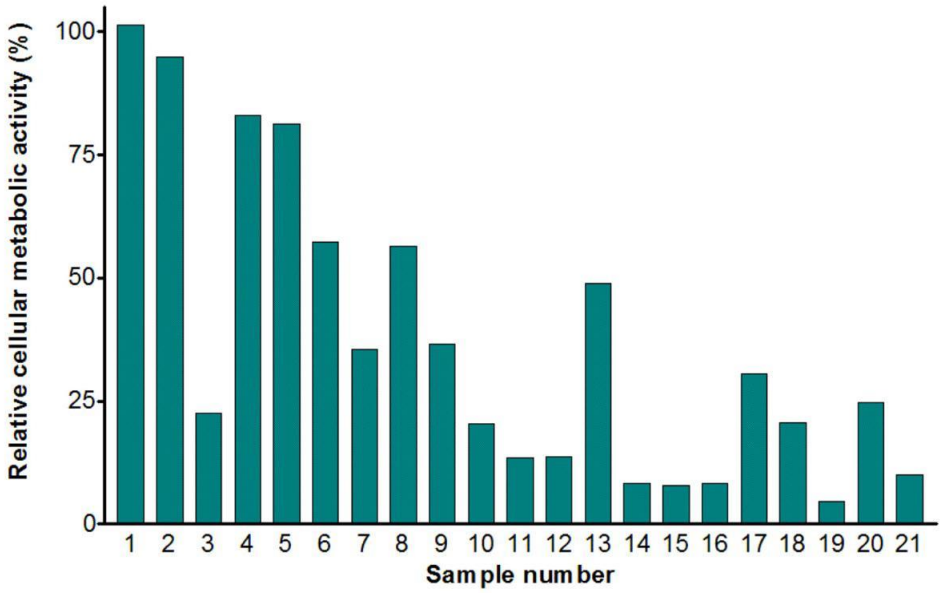

Figure 4. Sample viability. Sample viability prior to supernatant transfer onto Vero cells was determined by assessing cellular metabolic activity using a commercially available resazurin solution. Raw fluorescence values were normalized to that of untreated, uninfected wells.

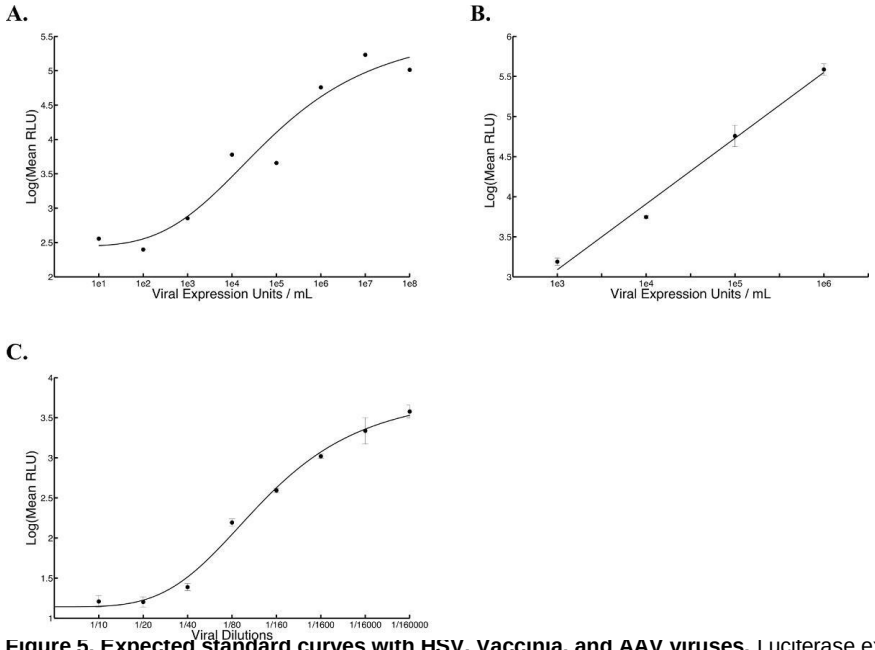

Figure 5. Expected standard curves with HSV, Vaccinia, and AAV viruses. Luciferase expression was measured at five different points within a well using a luminometer and bioluminescence was expressed in mean relative light units (RLU). **(A)** HSV standard curve was added onto Vero cells plated 24 hr earlier at a density of 2.5 x 10^4 cells per well (100 µl) and luciferase measurement was made 17 hr post supernatant transfer (R^2= 0.9489, n=1). A Hill equation was generated by solving the non-linear regression. **(B)** Vaccinia standard curve was added onto Vero cells plated 24 hr earlier a density of 2.5 x 10^4 cells per well (100 µl) and incubated for 2.5 hr at 37 °C, after which luciferase measurements were taken (R^2= 0.9892). A linear equation was generated by solving for the linear regression. **(C)** AAV standard curve was added onto human lung carcinoma cells (A549) plated 24 hr earlier at a density of 2.5 x 10^4 cells per well (100 µl) and luciferase measurement was made 24 hr post infection. A Hill equation was generated by solving the non-linear regression. The average of five replicate curves and standard error bars are shown (R^2= 0.9926).

Discussion

The luciferase-based approach described here provides a number of advantages over other existing methods including its ease, quickness, minimal equipment need, and relatively low cost. A key contributor to this is the avoidance of a serial dilution step. Nonetheless, serial dilution-

based derivatives of this protocol are certainly feasible and were recently used to assess luciferase-expressing Ebola titers in a high-throughput antiviral screen[11]. While inherently more time consuming and more expensive, such adaptations may provide greater dynamic range for viral quantification when necessary. In addition to being particularly well suited for evaluating viral titers in the context of high-throughput screens, our one-step luciferase based viral quantification method generates accurate estimates of infectious virions in the case of replicating viruses. Furthermore, readouts of luminescence along with cytotoxicity data from the same experiment give a more complete picture of the effect of the experimental conditions on target cells, which is particularly useful in the context of oncolytic viruses and drug screens.

The example illustrated here uses a replicating negative single strand RNA virus; however, this protocol can be adapted to a number of replicating and non-replicating viruses with a few minor protocol adjustments. This includes DNA viruses such as Vaccinia, HSV, and AAV (see **Figure 5**). Samples infected with intracellular viruses, such as Vaccinia virus for example, require a virus-release step prior to quantification (*e.g.*, at least one freeze-thaw cycle). When applying this technique to other viruses, it is necessary to optimize the incubation time from the transfer
of the viral supernatant or lysate to the reading of the plates by the luminometer. This parameter will depend mainly on the replication cycle of the virus in the permissive cell line and the strength of the promoter driving luciferase expression. This is best done by using the full standard curve in the optimization step. To do this, one must infect the appropriate permissive cell line with various replicates of the prepared standard curve and read each replicate at a different time points post-transfer. Ideally, an incubation time point is chosen that leads to a linear relationship between LOG(RLU) and LOG(titer) spanning the expected sample titer range. For VSVΔ51-Fluc, this is typically from 10^4 pfu/ml -10^7 pfu/ml for a 5 hr incubation time. If lower or higher titers are expected from samples, one can simply increase or reduce the incubation time respectively. Alternately, samples may be diluted to fall within the range much as is done typically for ELISA.

As mentioned above, this method is well suited to perform high-throughput drug screens using drug libraries as most of the steps can be automated. Cells can be plated efficiently using an automated microplate dispenser, the drug library can be added using a 96-channel liquid handler, virus can be added using a microplate dispenser and plates read using an automated luminometer. In theory, this can also be adapted to 384-well or smaller formats; however, the limitation to this end is number of cells that can be plated, given fewer cells leads to a narrower range in the linearity of the LOG(RLU) to LOG(Titer) relationship. Finally, assessment of cell viability using resazurin or other metabolic dyes can be easily incorporated in the workflow, allowing for discrimination of cytotoxic compounds in antiviral screens or identification of compounds that lead to synergistic killing in combination with viruses[12]. Nevertheless, limitations of this method include the requirement of a luciferase transgene expressing virus, which is not always possible, and the availability of a sufficiently permissive cell line. However, it is likely possible to adapt the method for use with other reporter genes (*e.g.*, GFP) provided the reporter quantification method has a suitable linearity and signal to noise ratio. Overall, the described high-throughput method can be modified to suit many different viruses and tailored to diverse applications.

Disclosures

The authors have nothing to disclose.

Acknowledgements

Vanessa Garcia is funded by a Queen Elizabeth II Ontario Graduate Scholarship in Science and Technology and Cory Batenchuk by a Natural Sciences and Engineering Research Council fellowship.

References

1. Grigorov, B., Rabilloud, J., Lawrence, P., & Gerlier, D. Rapid titration of measles and other viruses: optimization with determination of replication cycle length. *PLoS One.* **6**, e24135, doi:10.1371/journal.pone.0024135 PONE-D-11-10153 [pii] (2011).
2. Lizee, G. *et al.* Real-time quantitative reverse transcriptase-polymerase chain reaction as a method for determining lentiviral vector titers and measuring transgene expression. *Hum Gene Ther.* **14**, 497-507, doi:10.1089/104303403764539387 (2003).
3. McSharry, J. J. Uses of flow cytometry in virology. *Clin Microbiol Rev.* **7**, 576-604 (1994).
4. Watcharatanyatip, K. *et al.* Multispecies detection of antibodies to influenza A viruses by a double-antigen sandwich ELISA. *J Virol Methods.* **163**, 238-243, doi:10.1016/j.jviromet.2009.09.027 S0166-0934(09)00439-X [pii] (2010).
5. Dawson, E. Rapid, Direct Quantification of Viruses in Solution Using the ViroCyt Virus Counter. *Journal of Biomolecular Techniques.* **23**, S10 (2012).
6. Snyder, R. O. AAV and RT-PCR: true or false? *Mol Ther.* **1**, 389-390, doi:10.1006/mthe.2000.0066 S1525-0016(00)90066-2 [pii] (2000).
7. Diallo, J. S., Roy, D., Abdelbary, H., De Silva, N., & Bell, J. C. *Ex vivo* infection of live tissue with oncolytic viruses. *J Vis Exp.* (52), doi:10.3791/2854 2854 [pii] (2011).
8. Gaush, C. R., & Smith, T. F. Replication and plaque assay of influenza virus in an established line of canine kidney cells. *Appl Microbiol.* **16**, 588-594 (1968).
9. Green, M., & Loewenstein, P. M. Human adenoviruses: propagation, purification, quantification, and storage. *Curr Protoc Microbiol.* **Chapter 14**, Unit 14C 11, doi:10.1002/9780471729259.mc14c01s00 (2006).
10. Diallo, J. S., Vaha-Koskela, M., Le Boeuf, F., & Bell, J. Propagation, purification, and *in vivo* testing of oncolytic vesicular stomatitis virus strains. *Methods Mol Biol.* **797**, 127-140, doi:10.1007/978-1-61779-340-0_10 (2012).
11. Hoenen, T., Groseth, A., Callison, J., Takada, A., & Feldmann, H. A novel Ebola virus expressing luciferase allows for rapid and quantitative testing of antivirals. *Antiviral Res.* **99**, 207-213, doi:10.1016/j.antiviral.2013.05.017 S0166-3542(13)00157-5 [pii] (2013).

12. Diallo, J. S. *et al.* A high-throughput pharmacoviral approach identifies novel oncolytic virus sensitizers. *Mol Ther.* **18**, 1123-1129, doi:10.1038/mt.2010.67 mt201067 [pii] (2010).

